

THE NATURE OF E+A GALAXIES IN INTERMEDIATE REDSHIFT CLUSTERS^{1,2}KIM-VY H. TRAN³Department of Astronomy & Astrophysics, University of California, Santa Cruz, CA 95064
vy@phys.ethz.ch

MARIJN FRANX

Leiden Observatory, P.O. Box 9513, 2300 RA Leiden, The Netherlands
franx@strw.leidenuniv.nl

GARTH ILLINGWORTH

University of California Observatories/Lick Observatory, University of California, Santa Cruz, CA 95064
gdi@ucolick.org

DANIEL D. KELSON

Observatories of the Carnegie Institution of Washington, 813 Santa Barbara Street, Pasadena, CA, 91101
kelson@ociw.edu

PIETER VAN DOKKUM

Department of Astronomy, Yale University, New Haven, CT 06520-8101
dokkum@astro.yale.edu*Draft version November 1, 2018*

ABSTRACT

Combining HST/WFPC2 mosaics with extensive ground-based spectroscopy, we study the nature of E+A galaxies in three intermediate redshift clusters ($z = 0.33$, 0.58 , & 0.83). From a sample of ~ 500 confirmed cluster members, we isolate 46 E+A candidates to determine the E+A fraction and study their physical properties. Spectral types are assigned using Balmer ($H\delta$, $H\gamma$, $H\beta$) and $[OII]\lambda 3727$ equivalent widths. For all members, we have galaxy colors, luminosities, Hubble types, and quantitative structural parameters. We also include measured internal velocity dispersions for 120 cluster members, and estimate velocity dispersions for the rest of the cluster sample using the Fundamental Plane. We find E+A's comprise a non-negligible component (~ 7 – 13%) of the cluster population at these redshifts, and their diverse nature indicates a heterogeneous parent population. While cluster E+A's are predominantly disk-dominated systems, they span the range in Hubble type and bulge-to-total fraction to include even early-type members. Cluster E+A's also cover a wide range in luminosity ($L_B \sim 0.2$ – $2.5L_B^*$), internal velocity dispersion ($\sigma \sim 30$ – 220 km s $^{-1}$), and half-light radius ($r_{1/2} \sim 0.4$ – $4.3h^{-1}$ kpc). From their velocity dispersions and half-light radii, we infer that the descendants of E+A's in our highest redshift cluster are massive early-type galaxies. In contrast to the wide range of luminosity and internal velocity dispersion spanned by E+A's at higher redshift, only low mass E+A's are found in nearby clusters, *e.g.* Coma. The observed decrease in the characteristic E+A mass is similar to the decrease in luminosity of rapidly star-forming field galaxies since $z \sim 1$, *i.e.* galaxy “down-sizing.” In addition, we argue our statistics imply that $\gtrsim 30\%$ of the E-S0 members have undergone an E+A phase; the true fraction could be 100% if the effects of E+A down-sizing, an increasing E+A fraction with redshift, and the conversion of spirals into early-types are also considered. Thus, the E+A phase may indeed be an important stage in the transformation of star-forming galaxies into early-type members.

Subject headings: galaxies: clusters: general — galaxies: evolution — galaxies: fundamental parameters — galaxies: structure — galaxies: high-redshift

1. INTRODUCTION

Post-starburst galaxies (“E+A”; Dressler & Gunn 1983) in clusters may provide the crucial link in the morphological transformation of spiral galaxies into the elliptical/S0 systems that dominate the cluster population at the current epoch (cf. Butcher & Oemler 1978). Characterized by strong Balmer absorption and little or no $[OII]\lambda 3727$ emission, E+A's also are referred to as k+a/a+k (Franx

1993; Poggianti et al. 1999; Dressler et al. 1999, hereafter D99) or $H\delta$ -strong galaxies (Couch & Sharples 1987; Couch et al. 1994). Despite the short window of visibility of the post-starburst phase (< 1.5 Gyr; Couch & Sharples 1987; Barger et al. 1996; Leonardi & Rose 1996), E+A members can contribute up to 20% of the total cluster population (D99), and have been found in virtually every spectroscopic cluster survey from $0 < z < 0.8$ (Dressler & Gunn

¹ Based on observations with the NASA/ESA Hubble Space Telescope, obtained at the Space Telescope Science Institute, which is operated by the Association of Universities for Research in Astronomy, Inc., under NASA contract NAS 5-26555.

² Based on observations obtained at the W. M. Keck Observatory, which is operated jointly by the California Institute of Technology and the University of California.

³ Current address: Institute for Astronomy, ETH Hönggerberg, CH-8093 Zürich, Switzerland

1983; Couch & Sharples 1987; Wirth et al. 1994; Caldwell et al. 1996; Balogh et al. 1999; Dressler et al. 1999; Poggianti et al. 1999; Tran 2002).

However, the fraction of E+A galaxies in intermediate redshift clusters ($0.2 < z < 0.8$) is still debated. The MORPHS survey estimated a high E+A fraction of $\sim 20\%$ (D99) while the CNOC1 survey found a much lower fraction of $\sim 2\%$ (Balogh et al. 1999, hereafter B99). These results conflict as to whether the *majority* of cluster members undergo an E+A phase, or if only a small fraction do. If the real E+A fraction in clusters is high, it can be an important constraint on how members have evolved. For example, the transformation of late-type spirals via a post-starburst episode may explain the high number of passive S0 galaxies seen in nearby clusters (Dressler & Gunn 1983; Couch & Sharples 1987).

Once a robust E+A sample in intermediate redshift clusters is established, more fundamental issues such as the nature of the parent population can be addressed. Past studies find that while E+A's are heterogeneous in morphology, they tend to have disks (Wirth et al. 1994; Couch et al. 1994; Caldwell & Rose 1997; Couch et al. 1998, D99). Rotation velocities determined for a small subset of cluster E+A's at $z \lesssim 0.3$ also show most of them are rotationally supported systems (Franx 1993; Caldwell et al. 1996; Kelson et al. 2000b, hereafter K00b). However, it has been suggested that many field E+A's and some cluster E+A's are the result of processes that would easily disrupt a disk, e.g. merging and/or strong galaxy-galaxy interactions (Belloni et al. 1995; Liu & Kennicutt 1995; Zabludoff et al. 1996). Whether cluster E+A's include even the most massive galaxies, as suggested by Wirth et al. (1994), remains an open question.

A more challenging but extremely interesting question is what the descendants of cluster E+A's are. To answer this question, diagnostics that are not likely to evolve strongly with redshift are needed, e.g. internal velocity dispersions (σ) and half-light radii ($r_{1/2}$). However, published work on E+A's that utilizes both σ and $r_{1/2}$ have been limited to clusters at $z \lesssim 0.3$ (Franx 1993; Caldwell et al. 1996; Kelson et al. 1997, 2000c, hereafter K00c). By applying a similar analysis to E+A's at higher redshifts ($z \gtrsim 0.3$), we can determine if even the most massive galaxies in nearby clusters had an E+A phase in their past. Only with a combination of deep spectroscopy and high resolution imaging can both these parameters be measured with confidence in intermediate redshift clusters.

In the field, Cowie et al. (1996) find the maximum luminosity of galaxies undergoing rapid star formation has decreased smoothly since $z \sim 1$. This evolution in the characteristic mass of the star-forming population, referred to as "down-sizing," reflects how mass assembled, i.e. more massive galaxies formed at higher redshift. Recent work in clusters suggest down-sizing also can play an important role in rich environments (Poggianti et al. 2001; Kodama & Bower 2001; Poggianti 2003). If this is the case, the luminosity and internal velocity dispersion distributions of cluster E+A's should evolve as a function of redshift. By determining if the characteristic mass of cluster galaxies undergoing the E+A phase evolves, we can provide additional compelling evidence for down-sizing in clusters.

The high fraction of E+A galaxies in clusters relative

to the field suggests that environment plays a significant role in producing E+A's (D99). For example, the E+A phase may be triggered by an external source such as the strong galaxy-galaxy interactions suggested by studies of field E+A's (Liu & Kennicutt 1995; Zabludoff et al. 1996). In addition to direct mergers (van Dokkum et al. 1999), the cluster environment provides numerous other external forces that could trigger an E+A phase, e.g. ram-pressure stripping (Gunn & Gott 1972), gas compression (Dressler & Gunn 1983), perturbation by the tidal field (Byrd & Valtonen 1990), and galaxy harassment (Moore et al. 1996). The more disruptive interactions would create morphological signatures that should be visible during the E+A lifetime. Examining the number of E+A's that show morphological signs of recent mergers or interactions can help isolate which interactions trigger the E+A phase in clusters. Also, by comparing their spatial distribution to cluster substructure, we can test if the global cluster environment is effective at producing E+A's, or if they are better correlated with local over-densities.

To address these issues, we must first overcome the inherent difficulty of isolating E+A galaxies. A statistically representative sample of members (> 100) in *each* cluster is needed so that the relatively few E+A galaxies can be identified. Membership confirmation and E+A selection can only be accomplished reliably by obtaining spectra. In addition, high resolution imaging is needed at these redshifts ($z > 0.3$) to determine physical properties such as structural parameters and morphological type. Only by pairing wide-field HST/WFPC2 imaging with deep ground-based spectroscopy can we adequately study the E+A galaxies in intermediate redshift clusters.

From extensive spectroscopic surveys of CL1358 ($z = 0.33$; Fisher et al. 1998), MS2053 ($z = 0.58$; Tran 2002), and MS1054 ($z = 0.83$; Tran et al. 1999; van Dokkum et al. 2000; Tran 2002), we select 46 E+A candidates from ~ 500 confirmed cluster members. Using HST/WFPC2 mosaics taken of each cluster (all to $R_{BCG} \sim 1h^{-1}$ Mpc), we measure the colors, magnitudes, half-light radii, bulge-to-total fractions, degree of galaxy asymmetry, and morphological type of the cluster members. With LRIS (Oke et al. 1995) on Keck, we also have measured internal velocity dispersions for 120 cluster members (Kelson et al. 1997; van Dokkum et al. 1998a; Kelson et al. 2001, 2003, K00b). With these measured dispersions, accurate colors, and the Fundamental Plane (Faber et al. 1987; Djorgovski & Davis 1987), we estimate velocity dispersions for the remainder of the sample. Using the E+A's that satisfy our strict selection criteria, we determine the E+A fraction in intermediate redshift clusters, identify characteristics of their parent population, address what the descendants of these galaxies can be, and discuss the likely down-sizing of this population.

A brief description of the HST/WFPC2 imaging and ground-based spectroscopy is provided in §2. We describe our E+A selection criteria and address the discrepancy in the cluster E+A fraction found by different surveys in §3. After identifying the cluster E+A population, we examine the nature of these systems in §4. We discuss their properties and evolution in §5, and present our conclusions in §6. Unless otherwise noted, we use $\Omega_M = 0.3$, $\Omega_\Lambda = 0.7$, and $H_0 = 100h \text{ km s}^{-1} \text{ Mpc}^{-1}$ in this paper.

2. SUMMARY OF OBSERVATIONS AND DATA

We select E+A galaxies from a large program studying three X-ray luminous clusters at $z = 0.33$, 0.58 , & 0.83 (Table 1, references therein). Our dataset combines HST/WFPC2 mosaics (each to $R_{BCG} \sim 1h^{-1}$ Mpc) of these clusters with extensive ground-based spectroscopy. From the spectroscopy, we determine spectral types for all members (Fisher et al. 1998; van Dokkum et al. 2000; Tran 2002) as well as measure internal kinematics for a subset (Kelson et al. 1997; van Dokkum et al. 1998a; Kelson et al. 2001, 2003, K00b). From over 1200 redshifts obtained in the three fields, we isolate ~ 500 cluster members. Here we describe briefly the spectra and photometry used in this paper.

2.1. Photometry

The three clusters were imaged by HST/WFPC2 in the F606W and F814W filters. The image reduction and photometry are detailed for CL1358, MS2053, and MS1054 in van Dokkum et al. (1998b), Hoekstra et al. (2000), and van Dokkum et al. (2000) respectively. Following the method outlined in van Dokkum & Franx (1996), we transform from the WFPC2 filter system to redshifted Johnson magnitudes using:

$$\begin{aligned} B_z &= F814W + a(F606W - F814W) + b \\ V_z &= F814W + c(F606W - F814W) + d \end{aligned} \quad (1)$$

where the constants $\{a, b, c, d\}$ for an E/S0 galaxy are

$$\begin{aligned} \{1.021, 0.524, 0.204, 0.652\} &\quad z = 0.33 \\ \{0.354, 0.923, -0.173, 0.959\} &\quad z = 0.58 \\ \{-0.077, 1.219, -0.524, 1.229\} &\quad z = 0.83 \end{aligned} \quad (2)$$

These apparent magnitudes correspond to integrating the galaxy's spectral energy distribution through the redshifted Johnson filter curves. Apparent magnitude then is converted to an absolute magnitude adjusted for passive evolution (M_{Be}) using the distance moduli in Table 1; here we account for simple fading, as determined from the Fundamental Plane ($\Delta \log(M/L) \propto -0.40z$; van Dokkum et al. 1998a).

In our analysis, we include Hubble types from Fabricant et al. (2000, 2003) who visually typed all members with $m_{814} < 22$. In the nomenclature adopted by these authors, the morphological types of $\{E, E/S0, S0, S0/Sa, Sa, Sb, Sc, Sd\}$ were assigned values of $\{-5, -4, -2, 0, 1, 3, 5, 7\}$; intermediate values of $\{-3, -1, 2\}$ were also used and mergers assigned a value of 99. In the following, we consider E-S0 galaxies as having $-5 \leq T \leq -1$, S0/a-Sa galaxies $0 \leq T \leq 1$, and spirals $2 \leq T \leq 15$.

2.2. Spectroscopy

In CL1358, spectra of 230 members were obtained at the WHT and MMT. Details of the target selection and spectral reduction are in Fisher et al. (1998, hereafter F98). Additional high resolution spectra were taken with LRIS (Oke et al. 1995) on the Keck Telescope to obtain internal velocity dispersions of 55 members (K00b). Keck/LRIS was also used to obtain redshifts and internal velocity dispersions for both MS2053 and MS1054. In MS2053 and MS1054, 150 and 130 members were confirmed respectively (Tran et al. 1999; van Dokkum et al. 2000; Tran

2002), and internal velocity dispersions for 29 and 26 members measured (Kelson et al. 1997; van Dokkum et al. 1998a; Kelson et al. 2003). Detailed explanations of the spectral reductions including the wavelength calibration, sky subtraction, and removal of telluric absorption can be found in the noted references.

The wavelength coverage for virtually all members in the three clusters includes [OII] $\lambda 3727$, the 4000 Å break, and Balmer lines ($H\delta$, $H\gamma$, & $H\beta$). The inclusion of these spectral features are of paramount importance as E+A galaxies are defined spectroscopically as having strong Balmer absorption and no [OII] $\lambda 3727$ emission (Dressler & Gunn 1983; Zabludoff et al. 1996; Balogh et al. 1999; Poggianti et al. 1999, D99). The bandpasses used to determine the equivalent widths of these features are listed in Table 2.

3. DEFINING E+A GALAXIES

3.1. E+A Selection Criteria

We select E+A galaxies from the three clusters in our sample (Table 1) as having $(H\delta + H\gamma)/2 \geq 4$ Å and no [OII] emission (> -5 Å). Although using all three Balmer lines to select E+A's is the most robust approach (Newberry et al. 1990), $H\beta$ is severely compromised by sky lines in MS1054 and so we do not include $H\beta$ in our selection criteria (see Table 3). Due to the wavelength coverage, we cannot determine the equivalent width of [OII] $\lambda 3727$ for $\sim 7\%$ and $\sim 4\%$ of members in MS2053 and MS1054 respectively; for these galaxies, only $H\delta$ and $H\gamma$ are used to determine their E+A status. This adds four E+A's (H3549, H2345, H1746, H408) to the MS2053 sample. The 46 cluster members that satisfy these criteria are shown in Fig. 1 and their physical characteristics are listed in Table 4.

Because the spectral quality varies for the three clusters, we define a magnitude limit ($M_{Be} \leq -19.1 + 5\log h$, $m_{814} \sim 21.9$) set by MS1054, the highest redshift cluster in our sample. For uniformity, we consider only members brighter than this cut when comparing the E+A population between the clusters. In selecting E+A's, we also apply a signal to noise cut ($S/N \geq 20$) on the $H\delta$ and $H\gamma$ fluxes. Only 14 of the 46 E+A candidates satisfy these strict selection criteria; these spectra are shown in Fig. 2.

An important point is that the spectroscopic criteria used to identify E+A galaxies vary depending on author, as can be seen in Table 3. The use of different thresholds and lines, e.g. only $H\delta$ versus a combination of Balmer lines, can produce different E+A fractions even within the same sample. The most robust approach is to use all three Balmer lines (cf. Newberry et al. 1990) and [OII] $\lambda 3727$ but, as noted earlier, this is not possible for our entire sample. Thus we restrict ourselves to using [OII] $\lambda 3727$ in combination with $H\delta$ and $H\gamma$. The only exceptions in our sample are 2053-3549 and 2053-2345. Although we do not have OII EQW's for these two E+A candidates, both have strong $H\beta$ absorption such that $(H\delta + H\gamma + H\beta)/3 > 4$ Å, and all three Balmer lines have $S/N > 20$. It is very unlikely that these two E+A candidates also have strong OII emission because in the CL1358 and MS2053 samples, $> 90\%$ of members with $(H\delta + H\gamma + H\beta)/3 > 4$ Å show no significant [OII] $\lambda 3727$ emission. We confirm 1054-6567's lack of OII emission from a lower S/N spectrum.

Figure 3 shows $(B - V)_z$ versus $(H\delta + H\gamma)/2$ for the cluster sample; morphological types are included (Fabricant et al. 2000, 2003). If we consider only the galaxies brighter than our imposed magnitude limit, the average color of E+A galaxies tends to be bluer than that of the early-type population in each cluster. As simple errors in the spectroscopy could not produce such a uniformly blue sample in all three clusters, the E+A fraction must be real and robust.

3.2. The E+A Fraction in Intermediate Redshift Clusters

For members brighter than our magnitude cut ($M_{Be} = -19.1 + 5\log h$), we obtain E+A fractions of $7 \pm 4\%$, $10 \pm 6\%$, and $13 \pm 5\%$ at $z = 0.33$, 0.58 , & 0.83 respectively (Table 5); note we apply our strict E+A selection criteria here. If we include all confirmed members in each cluster and include all E+A candidates, the fractions are $9 \pm 2\%$, $7 \pm 2\%$, and $16 \pm 3\%$. Errors are determined by assuming a Poisson distribution for the E+A galaxies.

Considering the low E+A fraction in Coma⁴ ($\lesssim 3\%$; Caldwell et al. 1993), these results show the E+A fraction evolves strongly with redshift. They also suggest the E+A fraction continues to increase at $z > 0.5$. However, larger samples at $z > 0.3$ are needed to determine if this increase is real or if the trend flattens at $z > 0.3$.

3.3. Comparison to CNOC1

As noted earlier, there is disagreement in the literature as to whether the E+A fraction in intermediate redshift clusters ($z \gtrsim 0.3$) is significantly higher than that of the field. Published cluster surveys ($0.3 < z < 0.6$) estimate cluster E+A fractions of $\sim 10 - 20\%$ (Belloni et al. 1995; Couch et al. 1998, D99). In contrast, B99 argue that the average cluster E+A fraction is negligible ($1.5 \pm 0.8\%$) at $z = 0.18 - 0.55$, and comparable to the field. Is it possible to reconcile these two remarkably different claims?

While both D99 and B99 spectroscopically select their E+A samples using $H\delta$ and $[\text{OII}] \lambda 3727$, B99 apply a correction that decreases their cluster E+A fraction. Recognizing that quiescent galaxies with low Balmer indices dominate the cluster populations, B99 argue measurement errors will automatically produce outliers that are classified as E+A's. To remove this artificial inflation, they correct the fraction of "raw" cluster E+A's from $4.4 \pm 0.7\%$ to $1.5 \pm 0.8\%$. Furthermore, B99 note that in CL1358 the E+A fraction determined by F98 ($4.7 \pm 1.9\%$) is remarkably similar to the uncorrected E+A fraction from their combined cluster sample ($4.4 \pm 0.7\%$). They suggest F98 overestimated the true fraction by not correcting for inclusion of spurious outliers.

We test B99's theory by focusing on CL1358, a cluster included in B99's analysis and spectroscopically surveyed by both CNOC1 (Yee et al. 1996) and F98. If a significant number of E+A's in this cluster are actually passive galaxies, many of the E+A's should be as red as the early-types. Figure 4 shows the distribution of color versus Balmer strength for cluster members taken from F98 and B99; note B99 use only $H\delta$ as their Balmer criterion while F98 use the average of $H\delta$, $H\gamma$, and $H\beta$ (Table 3).

While E+A's selected by B99 have a large spread in color and can be as red as the passive population, virtually all of the E+A's found by F98 are *bluer* than the passive early-types. Simple errors in the spectral indices could not produce such a uniformly blue sample, and so these cannot be spectroscopically passive galaxies mistaken as E+A's.

In comparing results from F98 and B99 for ~ 100 common members, we find significant offsets in $H\delta$ and $[\text{OII}]$ between the two surveys; this may explain the discrepancy in the E+A fractions. On average, $H\delta$ equivalent width values are smaller ($\sim 0.7 \text{ \AA}$) and $[\text{OII}]$ emission larger ($\sim 2 \text{ \AA}$) in B99 as compared to F98. Given the equivalent widths used to determine the E+A phase (see Table 3), these offsets can seriously affect the final E+A selection. For example, if the indices of F98 are transformed to the system of B99 and B99's selection criteria used, the fraction of E+A's in CL1358 as measured with F98's spectra decreases from 4.7% to 3.4% .

B99 may have been motivated to correct their cluster E+A fractions if large errors were associated with the CNOC1 $H\delta$ measurements. To determine if the CNOC1 errors are significantly larger than those of F98 for CL1358, we independently estimate the equivalent width errors of both samples by comparing them to the high signal-to-noise spectra of K00b. Using 27 members common to the three studies, we estimate the true formal errors for $H\delta$ in both B99 and F98 are comparable ($\sim 1.5 \text{ \AA}$). This value is much smaller than the $H\delta$ formal error of 2.8 \AA associated with the F98 sample and subsequently used by B99. Thus in CL1358, B99 overestimated the correction factor due to measurement errors.

To summarize, the discrepancy between B99 and F98 is due to 1) the systematic offsets in the spectral indices, *i.e.* B99's $H\delta$ EQW values are smaller and $[\text{OII}] \lambda 3727$ larger than F98's and 2) B99's overestimate of the correction due to measurement errors. As we have shown, the offsets in the spectral indices used to define the CNOC1 CL1358 E+A sample reduces the observed number of E+A's. This combined with B99's correction factor produces a very low cluster E+A fraction. The E+A fraction ($\sim 5\%$) in CL1358 measured by F98 using their stricter selection criteria is valid.

4. NATURE OF CLUSTER E+A GALAXIES

Having established that a significant fraction of E+A galaxies exists in clusters up to $z \sim 0.8$, we now examine their physical properties to determine what type of galaxies they are. In the following, values for quantitative structural parameters, *e.g.* bulge-to-total fraction (B/T), galaxy asymmetry (R_A), total residual (R_T), half-light radius ($r_{1/2}$), and bulge/disk scale length (r_e, r_d), were measured by fitting two-dimensional de Vaucouleurs bulge plus exponential disk surface brightness models to the galaxies (Tran 2002; Tran et al. 2003). The galaxy residuals R_A and R_T are measured by taking the difference between the HST images and best-fit $r^{1/4}$ bulge+exponential disk model; how the residuals are measured is explained more fully in Tran et al. (2003). Unless otherwise noted, we only consider cluster members above our magnitude cut

⁴ Note that Caldwell et al. (1993) selected E+A's using different selection criteria from a sample of predominantly early-type members. However, recent results from the WINGS survey (Poggianti et al. 2001; Poggianti 2003) confirm the low E+A fraction in Coma for members brighter than $M_v = -18.5$.

of $M_{Be} = -19.1 + 5\log h$, and only the E+A's that satisfy our strict selection criteria.

4.1. Morphology

In this sample, the cluster E+A's span the range in Hubble type (Fig. 5) and bulge-to-total fraction (Fig. 6) to include both spirals and E/S0's. However, the majority of E+A's have measurable disks, consistent with results from previous cluster E+A studies (Wirth et al. 1994; Couch et al. 1994; Caldwell & Rose 1997; Couch et al. 1998; Caldwell et al. 1999, D99). Their average bulge-to-total fraction of ~ 0.4 reflects their tendency to be disk-dominated systems.

This diverse range in B/T and Hubble type is similar to the heterogeneous morphologies found in studies of lower redshift cluster E+A's ($z \lesssim 0.3$; Couch et al. 1998; Caldwell et al. 1999). It also confirms suggestions in earlier studies that E+A's must have a wide variety of progenitors (Wirth et al. 1994; Zabludoff et al. 1996, D99). In addition, the earliest-type E+A's are in our most distant cluster. It may be that more massive cluster members, i.e. early-types, had their E+A phase at higher redshift.

4.2. Interactions & Mergers

The morphological variety of E+A galaxies suggests that they are triggered by an external source, e.g. via the strong galaxy-galaxy interactions or the tidal forces proposed in earlier studies (Liu & Kennicutt 1995; Belloni et al. 1995; Zabludoff et al. 1996; Caldwell et al. 1999). The cluster environment provides a plethora of possible disruptive mechanisms, e.g. ram-pressure stripping (Gunn & Gott 1972), gas compression (Dressler & Gunn 1983), perturbation by the cluster tidal field (Byrd & Valtonen 1990), and galaxy harassment (Moore et al. 1996). Also, the high merger fraction in MS1054 indicates galaxy-galaxy merging is possible between members with low relative velocities (van Dokkum et al. 1999). As these cluster E+A's are predominantly disk-dominated systems, the more disruptive interactions would create morphological signatures (e.g. Barnes & Hernquist 1992; Moore et al. 1998) that are visible during the E+A lifetime (~ 1.5 Gyr; Couch & Sharples 1987; Barger et al. 1996; Leonardi & Rose 1996). By examining the number of E+A's that are considered mergers and/or that have high galaxy residuals, we attempt to isolate which interactions, if any, are associated with the E+A phase.

To identify mergers, we use classifications from van Dokkum et al. (1999), Fabricant et al. (2000), and Fabricant et al. (2003). We consider high residual galaxies as those having a high degree of asymmetry ($R_A \geq 0.5$; Schade et al. 1995) and/or total residual ($R_T \geq 0.1$; Tran et al. 2001).

Despite MS1054's high merger fraction ($\sim 17\%$; van Dokkum et al. 1999), only two of the mergers are considered E+A's; no other E+A's in our sample are associated with mergers. Wirth et al. (1994) and D99 also observe a low incidence of mergers associated with cluster E+A's. We find only about half of the cluster E+A's have high galaxy residuals (Fig. 6). For comparison, the fraction of high residual E+A's is larger than that of early-types (E-S0; $< 15\%$) and even early-type spirals (S0/a-Sa; $\sim 30\%$) but less than that of cluster spirals ($\sim 80\%$). The num-

ber of cluster E+A's with prominent disks combined with only half the sample having high galaxy residuals suggests mergers are not the primary trigger of the E+A phase in cluster galaxies.

4.3. Color-Magnitude Diagram

Even though galaxies can be brightened significantly during the E+A phase (up to ~ 1.5 mag; Barger et al. 1996), E+A's in nearby clusters tend to be faint systems ($L \lesssim 0.4L^*$; Caldwell et al. 1999). However, past studies of intermediate redshift clusters find E+A's with $L > L^*$ (Wirth et al. 1994, D99). Here we determine if the cluster E+A's in this sample are as luminous as the brightest cluster members, and whether they also cover a wide luminosity range.

In Fig. 7, we show the color-magnitude (CM) distribution of all cluster members and E+A candidates; all cluster members, including the E+A candidates, have been corrected for simple passive evolution (§2.1). In all three clusters, we find bright E+A's ($M_{Be} \lesssim -19.1 + 5\log h$); half of the 14 robust E+A's are brighter than M_{Be}^* ($-19.5 + 5\log h$ at $z = 0.83$; Hoekstra et al. 2000). Even more striking are the very luminous E+A's at $z = 0.83$: these E+A's are up to a magnitude brighter than their lower redshift counterparts and cover a larger magnitude range. Note the cluster E+A's tend to be bluer than the red sequence. The E+A luminosity range, particularly at $z = 0.83$, only reinforces the conclusion that they have a heterogeneous parent population. The fact that the brightest E+A's in this sample are in our most distant cluster is additional evidence for down-sizing of the cluster E+A population.

4.4. Brightening During the E+A Phase

Simple models show that during the post-starburst phase, galaxies can be brightened up to 1.5 magnitudes in the optical (Newberry et al. 1990; Barger et al. 1996). For comparison, we place here observational constraints on ΔM_{Be} using the internal velocity dispersions (σ) acquired for 120 members and the Fundamental Plane (Djorgovski & Davis 1987; Faber et al. 1987, see Appendix). As demonstrated in e.g. Faber et al. (1987), residuals from the FP can be expressed as residuals in the M/L ratio. We find the $\log(M/L)$ residuals of the nine cluster E+A's with measured σ range from ~ -0.5 to ~ 0.3 (Fig. 8). Assuming E+A's fade until $\Delta \log(M/L) = 0$, we estimate cluster E+A's are brightened by as much as $\Delta M_{Be} \sim 1.25$ mag, with a median of 0.25 mag.

Assuming the E+A's at $z = 0.83$ redden and fade by ~ 0.25 mag by $z = 0.33$, the only galaxies in CL1358 in this luminosity and color range are E-S0's and S0/a-Sa's (Fig. 7). This suggests that some of the brightest early-type galaxies in nearby clusters had an E+A phase in their past.

4.5. Internal Velocity Dispersions

Having demonstrated that E+A's at higher redshift can be as luminous as the brightest cluster members (§4.3), we now determine if these brighter E+A's are also *massive* galaxies, or whether they are simply low luminosity/mass members that are temporarily brightened. By determining the E+A mass distribution, we can characterize what

the E+A progenitors are and also constrain what their descendants at lower redshift can be. To address this issue, diagnostics that are not likely to depend strongly on redshift are needed, *i.e.* internal velocity dispersions and half-light radii.

While half-light radii (\sim sizes) are measured fairly robustly from the WFPC2 imaging (Tran et al. 2003), determining internal velocity dispersions (σ) at these redshifts is challenging. However, we have obtained direct σ measurements for 120 cluster members (Kelson et al. 1997; van Dokkum et al. 1998a; Kelson et al. 2001, K00b). With the colors, effective radii⁵, luminosities, and measured dispersions, we estimate velocity dispersions for the rest of the cluster sample using the Fundamental Plane. In this method, we correct M/L ratios of later-type members and essentially evolve them onto the color-magnitude relation defined by the early-types; see the Appendix for a detailed explanation of this method.

Figure 9 shows the distribution of internal velocity dispersions (measured and estimated σ) for cluster members brighter than our magnitude cut. The range in velocity dispersion for E+A galaxies increases at higher redshift: E+A's at $z = 0.33$ have smaller velocity dispersions ($\sigma \lesssim 150 \text{ km s}^{-1}$) than at $z = 0.58$ ($\sigma \lesssim 200 \text{ km s}^{-1}$) and $z = 0.83$ ($\sigma \lesssim 250 \text{ km s}^{-1}$). The difference between $z = 0.33$ and $z = 0.83$ is most striking. Considering the robustness of the spectroscopic data and high quality of the WFPC2 imaging, any E+A's with $\sigma > 200 \text{ km s}^{-1}$ (measured or estimated) in the two lower redshift clusters would have been easily detected *if they existed*.

To emphasize the disparity between the three clusters, we compare their half-light radii to internal velocity dispersions in Fig. 10; neither of these parameters is expected to evolve significantly within the redshift range covered here. For comparison, we also include E+A's from Coma using velocity dispersions from Caldwell et al. (1996) and half-light radii from Scudeggio et al. (1998). The half-light radii and dispersions of E+A's at $z = 0.83$ are comparable to those of the massive early-type members in all three clusters. In contrast, none of the E+A's at $z = 0.33$ nor in Coma could be considered a cluster giant. It is apparent that the progenitors of the lower redshift E+A's are very different from those at $z = 0.83$. As with their luminosity, the E+A's with the highest internal velocity dispersions are found in our most distant cluster.

Another key result from our analysis is that in the lowest redshift cluster, we find no counterparts to the bright, high σ late-types found at $z = 0.83$. The $\sigma > 200 \text{ km s}^{-1}$ galaxies in MS1054 include S0/a-Sa's, E+A's, spirals, and mergers while the only galaxies in CL1358 with such high dispersions are E-S0's (Figs. 9 & 10). If we assume that, given their similar cluster dispersions (Table 1), CL1358 ($z = 0.33$) is an evolved version of MS1054 ($z = 0.83$), then the wide mix of high σ systems in MS1054 must be morphologically transformed into E-S0's within ~ 2.5 Gyr. The E+A phase may be an integral step in this process.

⁵ To estimate velocity dispersions, we fit a pure de Vaucouleurs profile to the members instead of our normal de Vaucouleurs bulge+exponential disk.

⁶ We consider the regular cluster population to follow the luminosity functions determined from weak-lensing studies by Hoekstra et al. (1998, 2000, 2002). Here members were photometrically selected to have color deviations of < 0.2 mags from the color-magnitude relation normalized to early-type members.

4.6. Spatial Distribution & Substructure

The E+A's in our sample are found at R_{BCG} of $\sim 100 - 900 h^{-1}$ kpc (Fig. 11). Like D99, we find that E+A's tend to avoid the inner cluster core ($R_{BCG} \lesssim 100 h^{-1}$ kpc). At $z = 0.83$, three of the eight E+A's are associated with a large subcluster (> 20 members; Tran 2002), while at $z = 0.58$ the E+A's are found in both the main cluster and massive subcluster (Fig. 11, middle right). This suggests that $\sim 30\%$ of E+A's, if not more, are associated with the groups that are being accreted by the clusters.

5. DISCUSSION

In the following section, we attempt to form a coherent picture of the cluster E+A population at intermediate redshifts. Using the physical properties detailed in §4, we determine if E+A's would be equally as numerous in a mass selected sample and test if E+A's are drawn from the same parent population as regular cluster members⁶, and establish a connection between the progenitors and descendants of these systems.

As in §4, we only consider cluster members brighter than $M_{Be} = -19.1 + 5\log h$, and E+A's that satisfy our strict selection criteria (§3.2). One possible concern is how the varying richness of the three clusters affects the conclusions drawn from these data. However, we emphasize it is the relative number of spectra that is important. Our large sample of confirmed cluster members ($> 120/\text{cluster}$) combined with the extensive spectroscopic and photometric properties we have gathered allows us to make a meaningful analysis of the cluster E+A population.

5.1. Luminosity vs. Mass Selected E+A Sample

We find the fraction of E+A galaxies in intermediate redshift clusters ranges from 7 – 13% (Table 5). However, we note our spectroscopic survey is magnitude limited. From §4.4, we know E+A's can be brightened by as much as $\Delta M_{Be} \sim 1.25$ mag, and so the E+A fraction in a *mass selected* cluster sample might be lower. Here we determine the influence of brightening on the E+A fraction and estimate a mass selected fraction.

We first use the Schechter luminosity function (Schechter 1976) to populate cluster members as a function of magnitude; at $z = 0.83$, $M_{Be}^* = -19.5 + 5\log h$ mag and $\alpha = -1$ (Hoekstra et al. 2000). Since E+A's are brightened by $< \Delta M_{Be} >_{med} = 0.25$ mag (see §4.4), they follow a luminosity function with $M_{Be}^* = -19.75$ mag. By combining the two luminosity functions, we can estimate approximately how biased a luminosity selected sample is (Fig. 12). Note this approach assumes 1) all E+A's are brightened by 0.25 mags and 2) E+A's have the same α as regular cluster members. If 10% of the members are E+A's, *i.e.* if the total cluster luminosity function comprises 90% regular and 10% brightened, we estimate the E+A fraction in a luminosity selected sample ($M_{Be} \leq -19.1 + 5\log h$) is $\sim 1/3$ larger than that of a mass selected sample. Depending on the magnitude limit,

the E+A fraction in a mass selected sample can differ by $\sim 30\%$ compared to a magnitude selected fraction.

5.2. Progenitors and Descendants

In Coma, known E+A's are low luminosity ($L < 0.4L^*$), low dispersion ($\sigma < 150 \text{ km s}^{-1}$) systems that are unlikely to evolve into massive early-type members (Caldwell et al. 1996, 1999; Poggianti 2003). However, we find this is not the case at $z > 0.3$. From Figs. 9 & 10, we see that at $z = 0.33$, E-S0's and S0/a-Sa's are the only logical descendants of the high dispersion ($\sigma > 150 \text{ km s}^{-1}$) E+A's at $z = 0.83$. The E+A phase may signify the transformation of early-type spirals into E-S0's, and strongly star-forming spirals into S0/a-Sa's.

The young stellar ages implied by the E+A phase may seem to conflict with the old stellar ages ($z_f > 2$) derived from studies using the FP and absorption line strengths (Kelson et al. 1997; van Dokkum et al. 1998a; Kelson et al. 2001). However, these ages represent the mean epoch of star formation and do not preclude activity at $z < 2$. Furthermore, it is not clear whether all galaxies undergo the E+A phase. Also note that the total starburst population can be as little as 10% of the galaxy's final stellar mass (Barger et al. 1996). Assuming the majority of their stars formed at $z_f > 2$, even early-type members can be E+A's.

The connection between E+A progenitors and descendants agrees very well with the concept of "progenitor bias" introduced by van Dokkum & Franx (2001). In this scenario, as many as 50% of present day early-type members are transformed from (later) galaxy types at $z < 1$. This morphological evolution is strongly supported by the likely transformation of the E+A's at $z = 0.83$ to early-type members by $z = 0.33$.

Additional evidence for morphological transformation is provided by the high dispersion ($\sigma > 250 \text{ km s}^{-1}$) S0/a-Sa members at $z = 0.83$ (Fig. 13). The *only* $z = 0.33$ counterparts to these systems are E-S0 members. Although red early-type spirals have been observed in lower redshift clusters, e.g. Bower et al. (1992) and K00b, none have dispersions as high as those in MS1054.

5.3. E+A "Down-sizing"

In our cluster E+A sample, we find a trend of decreasing luminosity and internal velocity dispersion with decreasing redshift. This evolution is similar to the observed decrease since $z \sim 1$ in the maximum luminosity of field galaxies undergoing rapid star formation ("down-sizing"; Cowie et al. 1996). While a similar trend has also been suggested for clusters (Poggianti et al. 2001; Kodama & Bower 2001; Poggianti 2003), here we find compelling evidence that down-sizing applies directly to cluster E+A galaxies. The E+A's in our most distant cluster ($z = 0.83$) can be luminous (L up to $2.5L^*$) and can have high internal velocity dispersions ($\sigma > 200 \text{ km s}^{-1}$). In contrast, the E+A's in our lowest redshift cluster ($z = 0.33$) are $L \lesssim L^*$ and have low dispersions ($\sigma < 150 \text{ km s}^{-1}$). The data are such that if any bright, high dispersion E+A's existed in our lower redshift clusters, we would have detected them.

One possible concern is that we may be observing an evolution in the E+A *number fraction* rather than a real

evolution in mass (as traced by $\propto r_e \sigma^2$). If the E+A fraction increases with redshift, the likelihood of observing a luminous, high dispersion E+A also increases. With only three clusters, we cannot determine with certainty if the cluster E+A fraction continues to increase at $z > 0.3$, but we do note the E+A fraction is highest ($\sim 13\%$) in the $z = 0.83$ cluster.

5.3.1. Statistical Tests

We attempt to break the degeneracy between evolution in number fraction and in mass by comparing the E+A magnitude, velocity dispersion, and mass distributions to those of the spectroscopically confirmed cluster population. If E+A's are distributed like these other cluster members, we expect to find no difference in the E+A luminosity, velocity dispersion, and mass distributions when compared to the rest of the cluster members. Even if the E+A fraction evolves, this should be true at all redshifts. However, if we can establish that E+A's are distributed differently from the other cluster members, this would support evolution in mass.

In Fig. 14, we compare the luminosity, internal velocity dispersion, and mass ($\propto r_e \sigma^2$) distribution of spectroscopically confirmed cluster members to the E+A's (Fig. 14, left panels). Here we combine all three clusters to improve the statistics and use the non-parametric Kolmogorov-Smirnov (Press et al. 1992) and Wilcoxon tests (Siegel & Castellan 1988), and consider only members brighter than $M_{Be} = -19.1 + 5\log h$. Both tests find the E+A magnitude distribution to be indistinguishable from that of the members. Conversely, the same tests find the σ and mass distributions to be different with $\sim 90\%$ confidence. Although they can be as bright as the dominant early-types, the E+A's in this sample tend to have lower velocity dispersions and masses when compared to the rest of the cluster population.

Given we know galaxies are brightened during the E+A phase by as much as $\Delta M_{Be} \sim 1.25$ mag (§4.4), we note cluster E+A's would automatically be expected to have lower dispersions in a magnitude limited sample. To remove this possible bias, we now apply a velocity dispersion limit of $\sigma > 150 \text{ km s}^{-1}$ in addition to our magnitude limit (Fig. 14, right panels). Again, we find the luminosity distributions of E+A's and cluster members to be indistinguishable while their dispersion and mass distributions are different ($> 95\%$ CL for both). These results indicate the increase in cluster E+A luminosity and velocity dispersion with redshift reflects evolution in the E+A mass distribution rather than evolution in their number fraction.

To remove any possible bias introduced by spectroscopic incompleteness⁷, we now estimate a complete cluster sample by weighting each member by the inverse of the cluster's magnitude selection function (van Dokkum et al. 2000; Tran 2002). Here we assume the worst case scenario where the cluster sample is incomplete but the E+A sample is complete; in this case, we would expect the minimum difference between the two populations. As before, we consider only galaxies with $M_{Be} \leq -19.1 + 5\log h$ and $\sigma > 150 \text{ km s}^{-1}$. We find again a large difference between the two distributions of the velocity dispersions and masses (Fig. 15).

⁷ By $M_{Be} = -19.1 + 5\log h$, the completeness of the spectroscopic surveys drops to $\sim 60 - 70\%$.

We establish the significance of the difference by deriving the probability distribution of the D_{max} statistic in this modified K-S test from simulations. We assume that the parent populations are the same, but that the spectroscopically confirmed cluster sample suffers from incompleteness for which the counts are corrected. From 5000 realizations, we find that the probability of finding $D_{max} > D_{max}(\text{observed})$ is lower than 2% for both the velocity dispersion and mass distributions. Thus, it is very unlikely that the E+A's are drawn from the same parent population as the rest of the cluster members.

5.3.2. Independent Observational Evidence

We find additional evidence of mass down-sizing by combining our E+A sample with results from the literature (Fig. 16). While high σ E+A's are found in clusters up to $z \sim 1.3$ (van Dokkum & Stanford 2003), it seems only low σ ones exist in nearby clusters, e.g. Coma. We also find a trend of increasing σ with redshift in the range $0.02 < z < 1.27$. This increase in the characteristic E+A mass with redshift is consistent with the trend of increasing age with increasing velocity dispersion found in Coma early-types by Caldwell et al. (2003).

Note these results do not exclude lower σ E+A's at higher redshift, rather, lower σ E+A's simply fall below our strict selection criteria. Excellent examples of this point are E+A's 1358–343, 1358–481, and 2053–2081 (Table 4). Although fainter than our magnitude limit, all three have high S/N spectra and *measured* velocity dispersions $< 110 \text{ km s}^{-1}$.

5.4. Significance of the E+A Phase

Results from our study show that the E+A phase is not limited to a small fraction of predominately late-type members, but that many massive early-types also undergo this phase. To determine if a significant fraction of cluster early-types have had an E+A phase, we consider MS1054 ($z = 0.83$, $t_{age} \sim 6.5 \text{ Gyr}$, $H_0 = 70 \text{ km s}^{-1} \text{Mpc}^{-1}$). In this cluster, $\sim 8\%$ of the E-S0 members are also E+A's (see Fig. 5). To estimate a lower limit on the number of cluster E-S0's that have undergone an E+A phase by $z \sim 0.8$, we assume the E+A phase can occur at $z \lesssim 2.5$ ($t_{age} \sim 2.6 \text{ Gyr}$) and is visible for $\sim 1 \text{ Gyr}$. In this case, more than 30% of the E-S0's in MS1054 have had an E+A phase, with the restriction that we know of no E+A's with internal velocity dispersions $> 250 \text{ km s}^{-1}$.

However, the true number of early-types that have had an E+A phase can be easily 100% if we also consider 1) an increasing E+A fraction with redshift; 2) an increasing characteristic E+A mass with redshift; and 3) the conversion of spirals into early-types. For example, if the fraction of early-type E+A's increases to 15% at $z > 0.8$, the total number of cluster E-S0's that have undergone an E+A phase in MS1054 increases to $\sim 70\%$. As for the observed restriction that only E+A's with $\sigma < 250 \text{ km s}^{-1}$ exist at $z \lesssim 0.8$, an increasing characteristic mass may mean there is no upper mass limit on the E+A phenomenon at higher redshifts; even brightest cluster galaxies (BCG) may have had an E+A phase. In addition, morphological transformation is likely to play a prominent role in increasing the early-type E+A fraction. From comparing CL1358 to MS1054 (Fig. 9), we estimate $\sim 45\%$ of massive ($\sigma > 200 \text{ km s}^{-1}$) E-S0's are transformed from spirals;

even if only half of these undergo an E+A phase, the early-type E+A fraction increases by $\sim 20\%$. Any combination of these factors will only increase the number of E-S0's that have undergone an E+A phase.

Our estimates on the significance of the E+A phase depend heavily on how long the E+A phase is visible and whether E+A's evolve into early-types. However, even our conservative estimate of $\sim 30\%$ establishes the importance of the E+A phase for a non-negligible number of cluster E-S0's. If the true fraction is 100%, as we demonstrate it can be easily, the E+A phase would play a critical role in the transformation of spirals into the early-types that dominate the cluster population.

To confirm the importance of the E+A phase in the evolution of cluster galaxies, additional observations in this redshift regime and higher are needed. We suspect that more massive cluster members underwent an E+A phase at $z > 0.8$, but whether this also includes the BCG or if there is an upper mass limit to the E+A phase is unknown. For a cluster at $z \sim 1.3$, van Dokkum & Stanford (2003) find that the two brightest members show [OII] $\lambda 3727$ emission and enhanced $\text{H}\delta$ absorption; the fourth brightest cluster member is an E+A. Measuring OII and Balmer indices of BCG's at $0.8 < z < 1.3$ can establish if BCG's also undergo an E+A phase, and whether this transition occurs at $z \sim 1$. Another interesting possibility is to measure indices of $z > 1.5$ radio galaxies as they can be the predecessors of lower redshift BCG's (e.g. Venemans et al. 2002). With observations at higher redshift, we can determine if the E+A phase is related to the bulk of star formation, or if it is simply due to "frosting" by a small fraction of younger stars (Trager et al. 2000).

6. CONCLUSIONS

We estimate the E+A fraction in intermediate redshift clusters and examine the physical properties of this population using HST/WFPC2 mosaics and extensive ground-based spectroscopy. Our results are based on spectral types, galaxy colors, magnitudes, Hubble types, and quantitative structural parameters for ~ 500 confirmed members in three clusters ($z = 0.33$, 0.58 , & 0.83). We also include measured internal velocity dispersions for a subset of 120 members, and estimate dispersions for the rest of the cluster galaxies using the Fundamental Plane.

We find E+A's make up a non-negligible component of the cluster population ($\sim 7 - 13\%$) at intermediate redshifts. They tend to be bluer than the passive members, and we estimate the E+A phase can brighten a galaxy by as much as $\Delta M_{Be} \sim 1.25 \text{ mag}$. Although most of them are disk-dominated systems, E+A's span the range in morphological type to include even E-S0 members. They can be more luminous than L^* and can have internal velocity dispersions in excess of 200 km s^{-1} . The majority of these E+A's are not associated with mergers.

The diverse nature of E+A members indicates they are drawn from a heterogeneous parent population. The characteristics of their descendants can be equally varied; even massive early-type members may have had an E+A phase in their past. Our study indicates the high dispersion ($\sigma > 200 \text{ km s}^{-1}$) E+A's at $z = 0.83$ are the logical progenitors of massive early-types at lower redshift.

The cluster E+A's are distributed such that the most luminous, high dispersion ones are in our most distant cluster while only $L \lesssim L^*$, low dispersion E+A's exist in our lowest redshift cluster and Coma (Caldwell et al. 1996, 1999). The trend of increasing luminosity and internal velocity dispersion with redshift provides compelling evidence for mass evolution in the cluster E+A population. This galaxy "down-sizing" is similar to the observed decrease in luminosity of rapidly star-forming field galaxies since $z \sim 1$ (Cowie et al. 1996). Comparison of the E+A luminosity, velocity dispersion, and mass ($\propto r_e \sigma^2$) distributions to the rest of the cluster members indicate this evolution in the E+A mass distribution is real. However, we cannot completely rule out that the luminous, massive E+A's found at higher redshift are due only to an increasing E+A fraction.

Using statistical arguments, we find that $\gtrsim 30\%$ of cluster E-S0's at $z = 0.83$ have had an E+A phase. We consider this a lower limit as evolution in the E+A fraction and characteristic mass as well as the conversion of spirals into early-types can increase the true fraction to 100%. These results show that the E+A phase can play an important role in the transformation of star-forming galaxies into early-type members.

Recognizing that our study is based on only three clus-

ters, these results can only benefit from a similar analysis of other clusters within this redshift range ($0.3 < z < 0.8$). Also needed is a comparative study of intermediate z field E+A's to determine if field and cluster E+A's evolve in a similar manner. Previous studies on the field E+A fraction at $z > 0.2$ disagree (5% vs. $\sim 0.1\%$; Hammer et al. 1997, B99), and how the field E+A's evolve in luminosity and mass has yet to be determined. Using the considerable field sample we have acquired in our cluster survey, we will quantify and characterize the nature of field E+A's in a future paper.

We are indebted to M. Balogh for making available the CNOC1 data on CL1358. We appreciate the useful comments S. Faber and the referee provided on this manuscript. K. Tran thanks the Lorentz Institute for their generous hospitality during multiple visits. Support from NASA HST grants GO-07372-96A, GO-06745-95A, GO-05991-94A, and GO-05989-94A, and NASA grant NAG5-7697 is gratefully acknowledged. The authors thank the entire staff of the W. M. Keck Observatory for their support, and extend special thanks to those of Hawaiian ancestry on whose sacred mountain we are privileged to be guests.

REFERENCES

Balogh, M. L., Morris, S. L., Yee, H. K. C., Carlberg, R. G., & Ellingson, E. 1999, *ApJ*, 527, 54

Barger, A. J., Aragon-Salamanca, A., Ellis, R. S., Couch, W. J., Smail, I., & Sharples, R. M. 1996, *MNRAS*, 279, 1

Barnes, J. E. & Hernquist, L. 1992, *ARA&A*, 30, 705

Belloni, P., Bruzual, A. G., Thimm, G. J., & Roser, H.-J. 1995, *A&A*, 297, 61

Binney, J. & Tremaine, S. 1987, *Galactic Dynamics* (Cambridge: Princeton University Press)

Bower, R. G., Lucey, J. R., & Ellis, R. S. 1992, *MNRAS*, 254, 601+

Butcher, H. & Oemler, A. 1978, *ApJ*, 219, 18

Byrd, G. & Valtonen, M. 1990, *ApJ*, 350, 89

Caldwell, N. & Rose, J. A. 1997, *AJ*, 113, 492

Caldwell, N., Rose, J. A., & Dendy, K. 1999, *AJ*, 117, 140

—. 2003, *AJ*, astro-ph/0303345

Caldwell, N., Rose, J. A., Franx, M., & Leonardi, A. J. 1996, *AJ*, 111, 78+

Caldwell, N., Rose, J. A., Sharples, R. M., Ellis, R. S., & Bower, R. G. 1993, *AJ*, 106, 473

Couch, W. J., Barger, A. J., Smail, I., Ellis, R. S., & Sharples, R. M. 1998, *ApJ*, 497, 188

Couch, W. J., Ellis, R. S., Sharples, R. M., & Smail, I. 1994, *ApJ*, 430, 121

Couch, W. J. & Sharples, R. M. 1987, *MNRAS*, 229, 423

Cowie, L. L., Songaila, A., Hu, E. M., & Cohen, J. G. 1996, *AJ*, 112, 839

Djorgovski, S. & Davis, M. 1987, *ApJ*, 313, 59

Dressler, A. & Gunn, J. E. 1983, *ApJ*, 270, 7

Dressler, A., Smail, I., Poggianti, B. M., Butcher, H., Couch, W. J., Ellis, R. S., & Oemler, A. J. 1999, *ApJS*, 122, 51

Faber, S. M., Dressler, A., Davies, R. L., Burstein, D., & Lynden-Bell, D. 1987, in *Nearly Normal Galaxies. From the Planck Time to the Present*, 175–183

Fabricant, D., Franx, M., & van Dokkum, P. 2000, *ApJ*, 539, 577

—. 2003, in prep

Fisher, D., Fabricant, D., Franx, M., & van Dokkum, P. 1998, *ApJ*, 498, 195+

Franx, M. 1993, *PASP*, 105, 1058

Gunn, J. E. & Gott, J. R. I. 1972, *ApJ*, 176, 1

Hammer, F., Flores, H., Lilly, S. J., Crampton, D., Le Fevre, O., Rola, C., Mallen-Ornelas, G., Schade, D., & Tresse, L. 1997, *ApJ*, 481, 49

Hoekstra, H., Franx, M., & Kuijken, K. 2000, *ApJ*, 532, 88

Hoekstra, H., Franx, M., Kuijken, K., & Squires, G. 1998, *ApJ*, 504, 636

Hoekstra, H., Franx, M., Kuijken, K., & van Dokkum, P. G. 2002, *MNRAS*, 333, 911+

Im, M., Simard, L., Koo, D. C., Faber, S. M., Gebhardt, K., Willmer, C. N. A., Phillips, A., Illingworth, G., Vogt, N. P., & Sarajedini, V. L. 2001, *AJ*, 122, 750

Jorgensen, I., Franx, M., & Kjaergaard, P. 1996, *MNRAS*, 280, 167

Kelson, D. D., Illingworth, G. D., Franx, M., & van Dokkum, P. G. 2001, *ApJ*, 552, L17

—. 2003, in prep

Kelson, D. D., Illingworth, G. D., van Dokkum, P. G., & Franx, M. 2000a, *ApJ*, 531, 137

—. 2000b, *ApJ*, 531, 159

—. 2000c, *ApJ*, 531, 184

Kelson, D. D., van Dokkum, P. G., Franx, M., Illingworth, G. D., & Fabricant, D. 1997, *ApJ*, 478, L13

Kodama, T. & Bower, R. G. 2001, *MNRAS*, 321, 18

Leonardi, A. J. & Rose, J. A. 1996, *AJ*, 111, 182

Liu, C. T. & Kennicutt, R. C. 1995, *ApJ*, 450, 547

Moore, B., Katz, N., Lake, G., Dressler, A., & Oemler, A. 1996, *Nature*, 379, 613

Moore, B., Lake, G., & Katz, N. 1998, *ApJ*, 495, 139+

Newberry, M. V., Boroson, T. A., & Kirshner, R. P. 1990, *ApJ*, 350, 585

Oke, J. B., Cohen, J. G., Carr, M., Cromer, J., Dingizian, A., Harris, F. H., Labrecque, S., Luciano, R., Schaal, W., Epps, H., & Miller, J. 1995, *PASP*, 107, 375

Poggianti, B. M. 2003, Carnegie Cluster Symposium, astro-ph/0307091

Poggianti, B. M., Bridges, T. J., Mobasher, B., Carter, D., Doi, M., Iye, M., Kashikawa, N., Komiyama, Y., Okamura, S., Sekiguchi, M., Shimasaku, K., Yagi, M., & Yasuda, N. 2001, *ApJ*, 562, 689

Poggianti, B. M., Smail, I., Dressler, A., Couch, W. J., Barger, A. J., Butcher, H., Ellis, R. S., & Oemler, A. 1999, *ApJ*, 518, 576

Press, W. H., Teukolsky, S. A., Vetterling, W. T., & Flannery, B. P. 1992, *Numerical recipes in FORTRAN. The art of scientific computing* (Cambridge: University Press, —c1992, 2nd ed.)

Schade, D., Lilly, S. J., Crampton, D., Hammer, F., Le Fevre, O., & Tresse, L. 1995, *ApJ*, 451, L1

Schechter, P. 1976, *ApJ*, 203, 297

Scodellato, M., Giovanelli, R., & Haynes, M. P. 1998, *AJ*, 116, 2728

Siegel, S. & Castellan, N. J. 1988, *Nonparametric Statistics for the Behavioral Sciences* (McGraw-Hill)

Trager, S. C., Faber, S. M., Worthey, G., & González, J. J. 2000, *AJ*, 120, 165

Tran, K. H. 2002, PhD thesis, Univ. California at Santa Cruz

Tran, K. H., Kelson, D. D., van Dokkum, P., Franx, M., Illingworth, G. D., & Magee, D. 1999, *ApJ*, 522

Tran, K. H., Simard, L., Illingworth, G. D. I., & Franx, M. 2003, *ApJ*, in press

Tran, K. H., Simard, L., Zabludoff, A. I., & Mulchaey, J. S. 2001, *ApJ*, 549, 172

van Dokkum, P. G. & Franx, M. 1996, *MNRAS*, 281, 985

—. 2001, *ApJ*, 553, 90

van Dokkum, P. G., Franx, M., Fabricant, D., Illingworth, G. D., & Kelson, D. D. 2000, *ApJ*, 541, 95

van Dokkum, P. G., Franx, M., Fabricant, D., Kelson, D. D., & Illingworth, G. D. 1999, *ApJ*, 520, L95

van Dokkum, P. G., Franx, M., Kelson, D. D., & Illingworth, G. D. 1998a, *ApJ*, 504, L17

van Dokkum, P. G., Franx, M., Kelson, D. D., Illingworth, G. D., Fisher, D., & Fabricant, D. 1998b, *ApJ*, 500, 714+

van Dokkum, P. G. & Stanford, S. A. 2003, *ApJ*, 585, 78

Venemans, B. P., Kurk, J. D., Miley, G. K., Röttgering, H. J. A., van Breugel, W., Carilli, C. L., De Breuck, C., Ford, H., Heckman, T., McCarthy, P., & Pentericci, L. 2002, *ApJ*, 569, L11

Wirth, G. D., Koo, D. C., & Kron, R. G. 1994, *ApJ*, 435, L105

Yee, H. K. C., Ellingson, E., & Carlberg, R. G. 1996, *ApJS*, 102, 269+

Zabludoff, A. I., Zaritsky, D., Lin, H., Tucker, D., Hashimoto, Y., Shectman, S. A., Oemler, A., & Kirshner, R. P. 1996, *ApJ*, 466, 104+

Higher resolution version of this
figure available at:

www.exp-astro.phys.ethz.ch/tran

FIG. 1.— Color images made with WFPC2 F814W and F606W imaging of the 46 E+A candidates from our cluster sample. The images are $10'' \times 10''$ (CL1358, $z = 0.33$), $7'' \times 7''$ (MS2053, $z = 0.58$), and $5'' \times 5''$ (MS1054, $z = 0.83$). Members are ordered by decreasing M_{Be} , and the 14 E+A's above our magnitude and S/N cut are noted with an asterix. For comparison, a representative bright elliptical member is included for each cluster: they are 1358-256, 2053-1993, and 1054-5450. (F606W-F814W) corresponds closely to redshifted ($B - V$) and ($U - B$) for CL1358 and MS1054 respectively; it falls between the two colors for MS2053.

Higher resolution version of this
figure available at:

www.exp-astro.phys.ethz.ch/tran

FIG. 2.— Smoothed spectra of the 14 E+A galaxies that satisfy our stringent selection criteria. The vertical dotted lines denote the bandpass for [OII] $\lambda 3727$, H δ , H γ , and H β . Note the strong absorption of all three Balmer lines for E+A's in CL1358 and MS2053; H β measurements in MS1054 are severely compromised by sky lines. For 1054-6567, lack of OII $\lambda 3727$ emission is confirmed from a lower S/N spectrum.

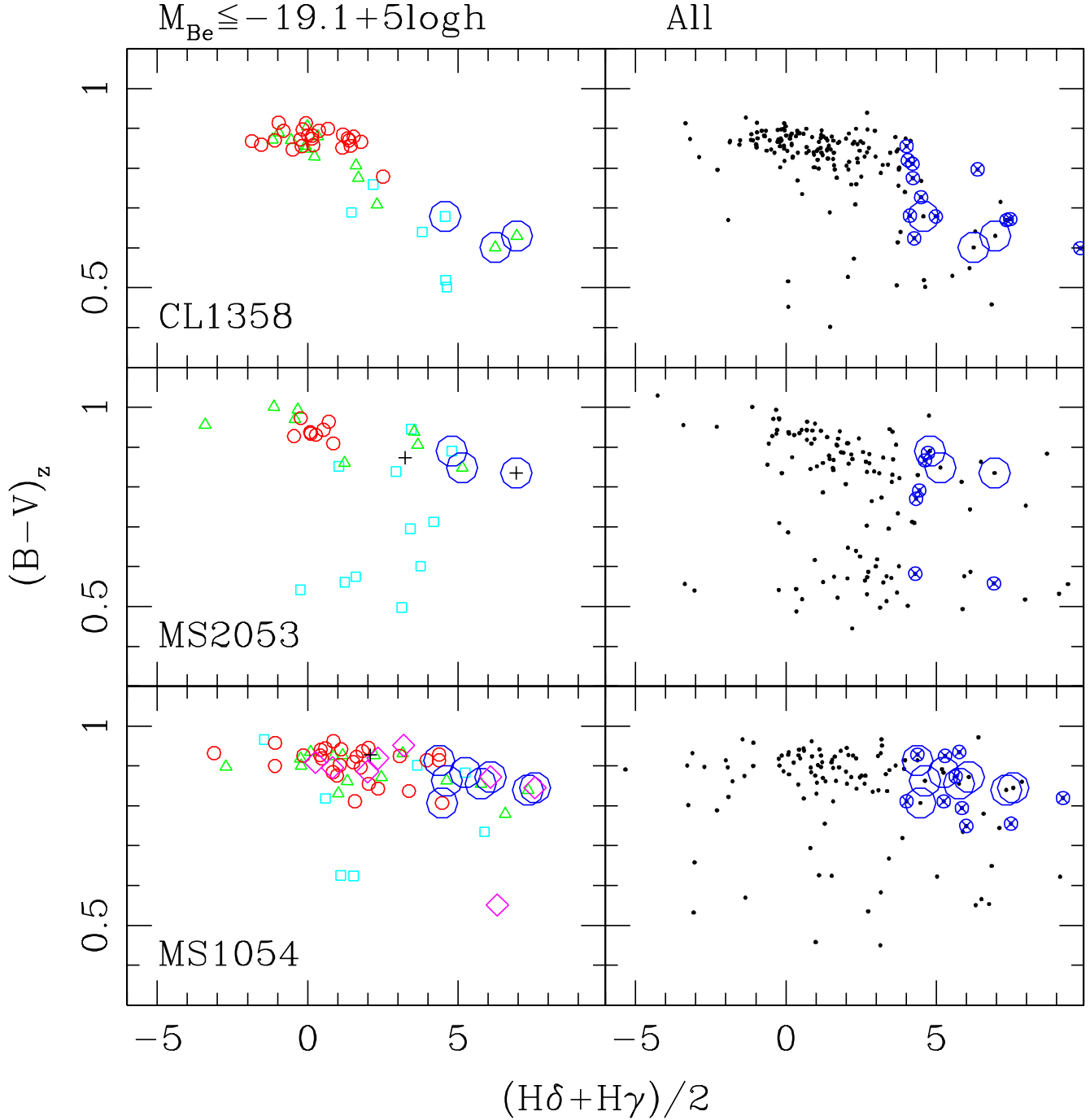


FIG. 3.— *Left:* Comparison of $(B-V)_z$ versus Balmer absorption [defined here as $(H\delta+H\gamma)/2$] for all members brighter than $M_{Be} = -19.1 + 5\log h$ in CL1358 ($z = 0.33$; top), MS2053 ($z = 0.58$; middle), and MS1054 ($z = 0.83$; bottom). The symbols represent different morphological types: E-S0 (small open circles), S0/a-Sa (open triangles), spiral (open squares), no type (plus signs), merger (diamonds), and E+A (large open circles). E+A's tend to be bluer than the early-type members. *Right:* The same comparison except now with all the confirmed cluster members. Circles with crosses denote E+A candidates fainter than our adopted magnitude limit ($M_{Be} = -19.1 + 5\log h$) and/or with spectral $S/N < 20$.

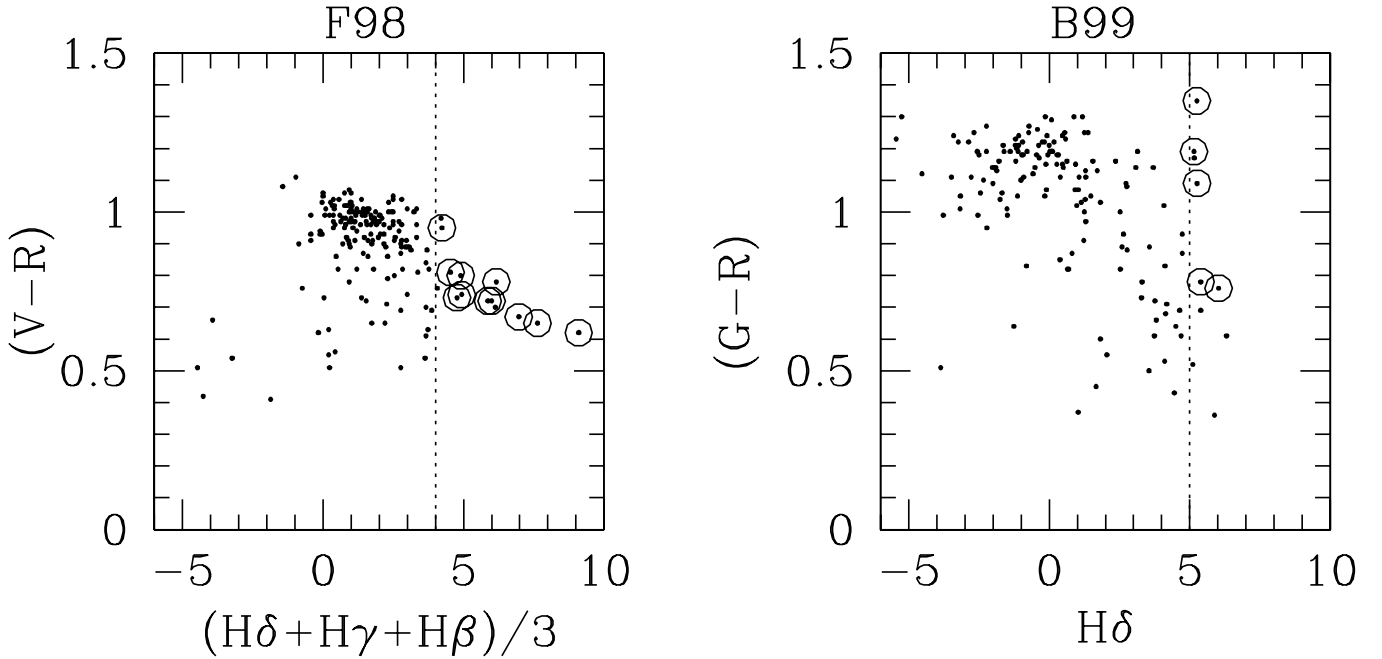


FIG. 4.— Color versus Balmer strength for CL1358 members surveyed by F98 (left) and B99 (right); F98 and B99 used different ground-based filter systems. Large open circles are E+A galaxies as defined in their respective surveys. The two groups differ in how they define Balmer strength: F98 take the average of $H\delta$, $H\gamma$, and $H\beta$ while B99 only use $H\delta$ (Table 3). The vertical dotted lines denote the Balmer cut-off for each survey. With only one exception, E+A galaxies as defined by F98 are systematically *bluer* than the passive members. In contrast, E+A galaxies selected by B99 span the range in color. The E+A sample as determined by F98 is robust and demonstrates that E+A's make up a non-negligible fraction of cluster members ($\gtrsim 5\%$).

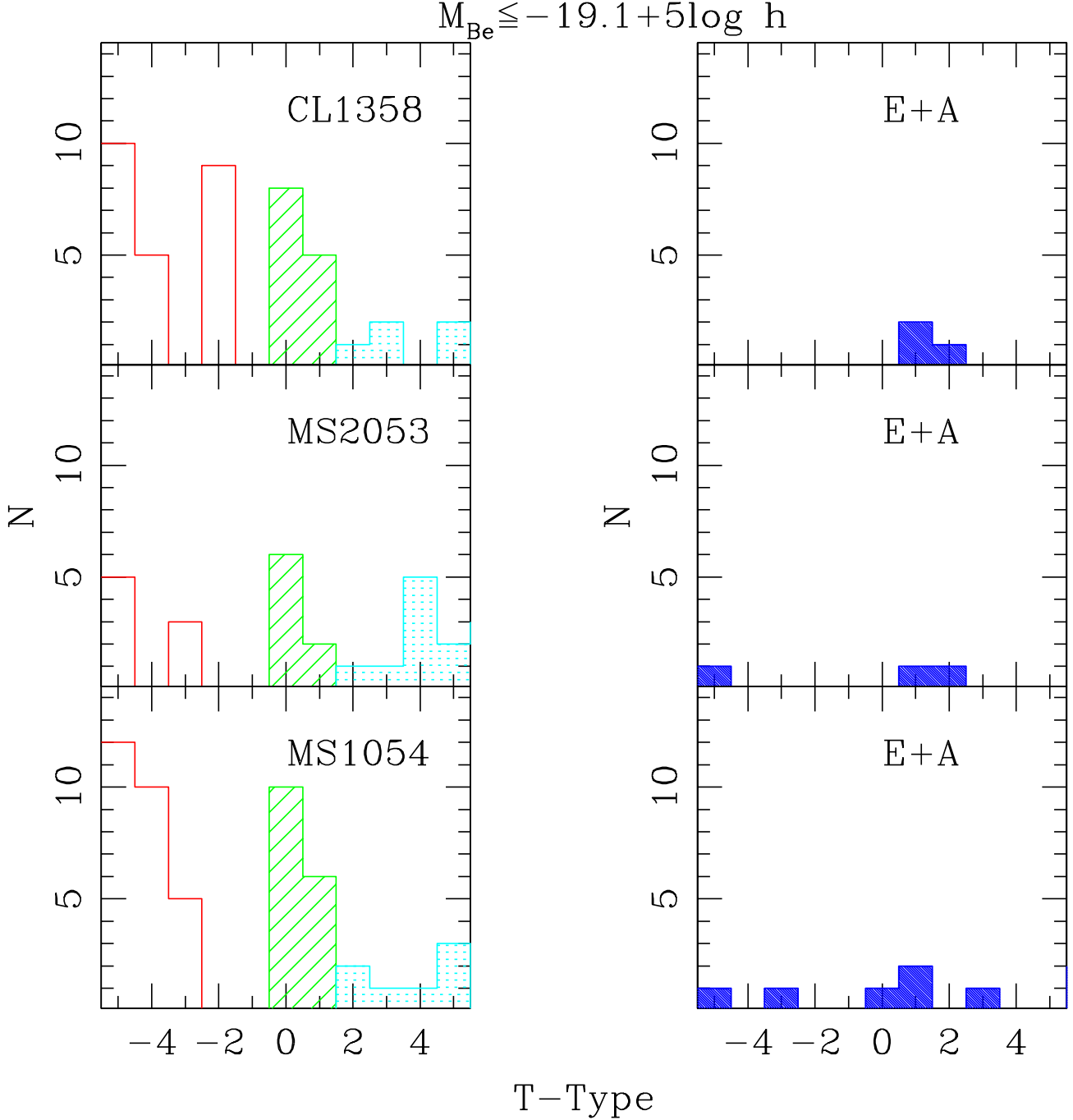


FIG. 5.— Histograms of Hubble type for cluster members above our magnitude limit. In the left panels, open regions correspond to E-S0's ($-5 \leq T \leq -1$), hatched regions to S0/a-Sa's ($0 \leq T \leq 1$), and dotted regions to spirals ($T \geq 2$). The respective E+A distributions of the three clusters are shown in the right panels; two of the E+A's in MS1054 are considered mergers (not shown). The E+A galaxies span the range of morphological type but tend to be systems with disks.

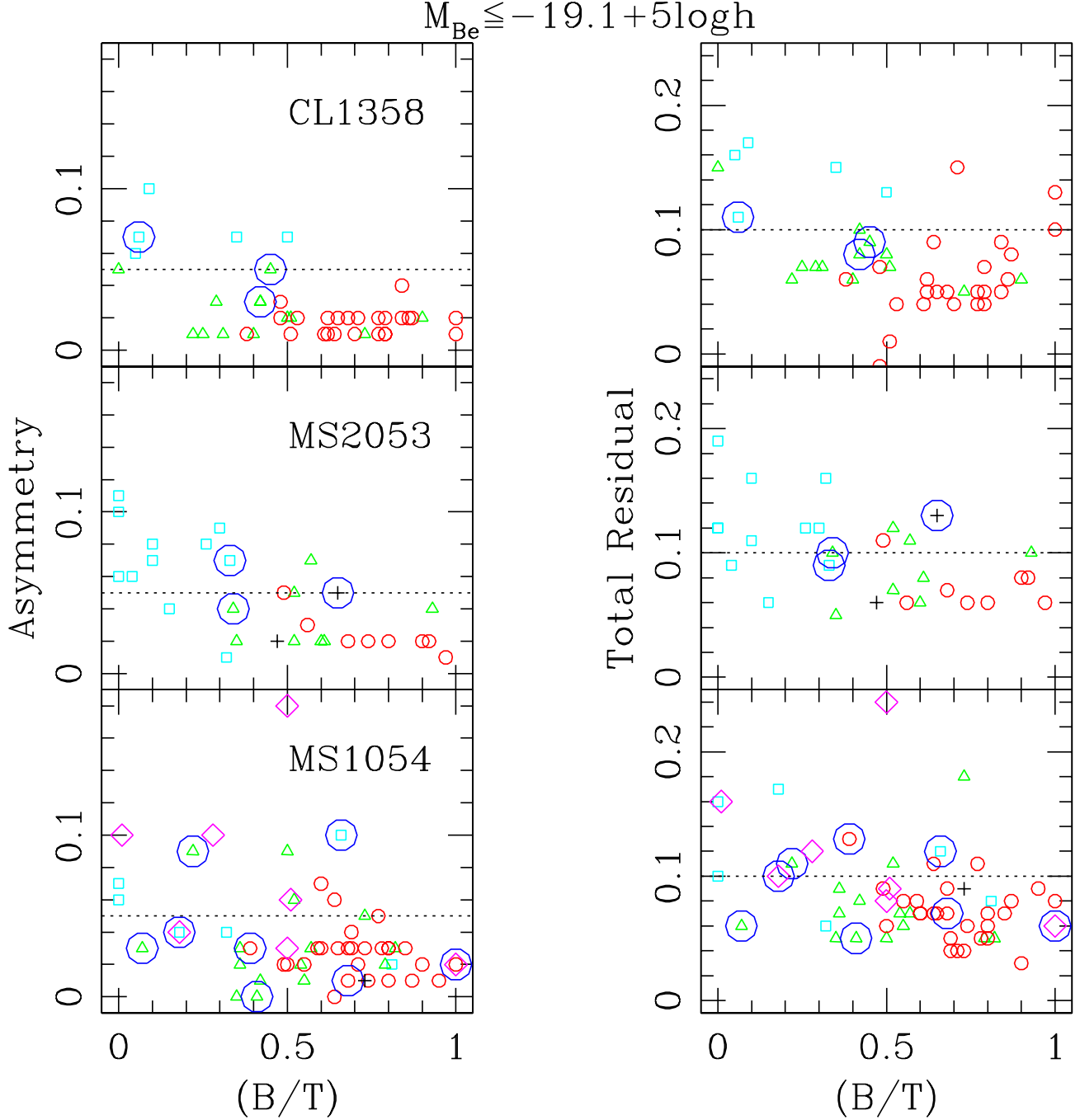


FIG. 6.— Comparison of galaxy asymmetry (R_A ; left panels) and total residual (R_T ; right panels) to bulge fraction (B/T) determined from a de Vaucouleurs bulge+exponential disk profile. Typical systematic errors for R_A , R_T , and B/T are ~ 0.02 , 0.02 , & 0.10 respectively (Im et al. 2001; Tran 2002; Tran et al. 2003). Again, only galaxies above our magnitude cut are shown. Approximately 40–50% are considered high residual galaxies, *i.e* having either $R_A = 0.05$ or $R_T = 0.1$; these limits are denoted by dotted horizontal lines. E+A's span the range in B/T but the majority of them have $(B/T) < 0.7$, meaning they have a measurable disk component.

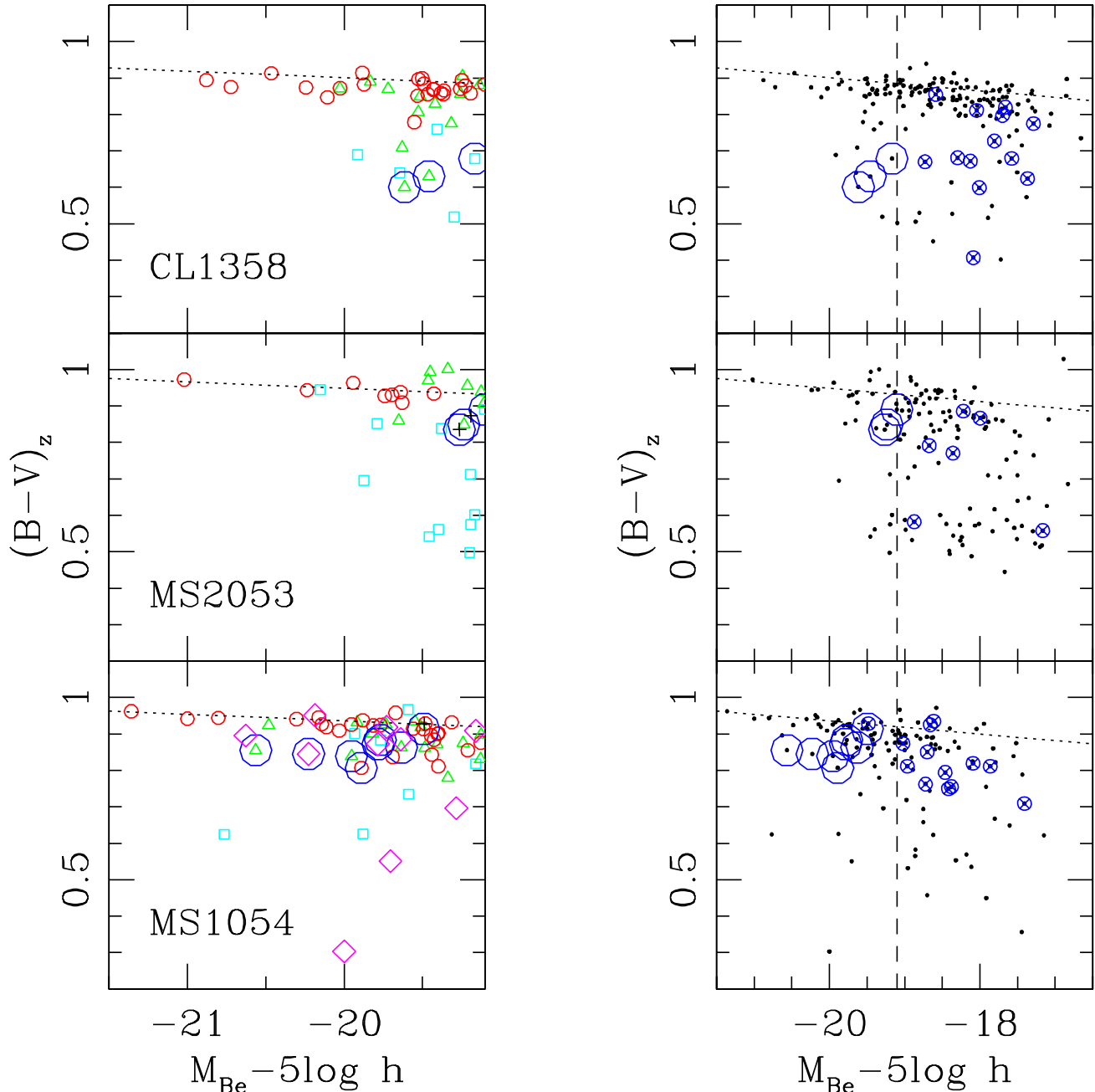


FIG. 7.— The left panels show the color-magnitude diagram for members with $M_{Be} \leq -19.1 + 5\log h$ while the right panels show all confirmed cluster members (symbols are as in Fig. 3). The color-magnitude relation (dotted line) is normalized to the E-S0 members and its slope is from van Dokkum et al. (2000). E+A galaxies in the two lower redshift clusters are faint ($M_{Be} \gtrsim -19.5 + 5\log h$) but can be up to a magnitude brighter in MS1054.

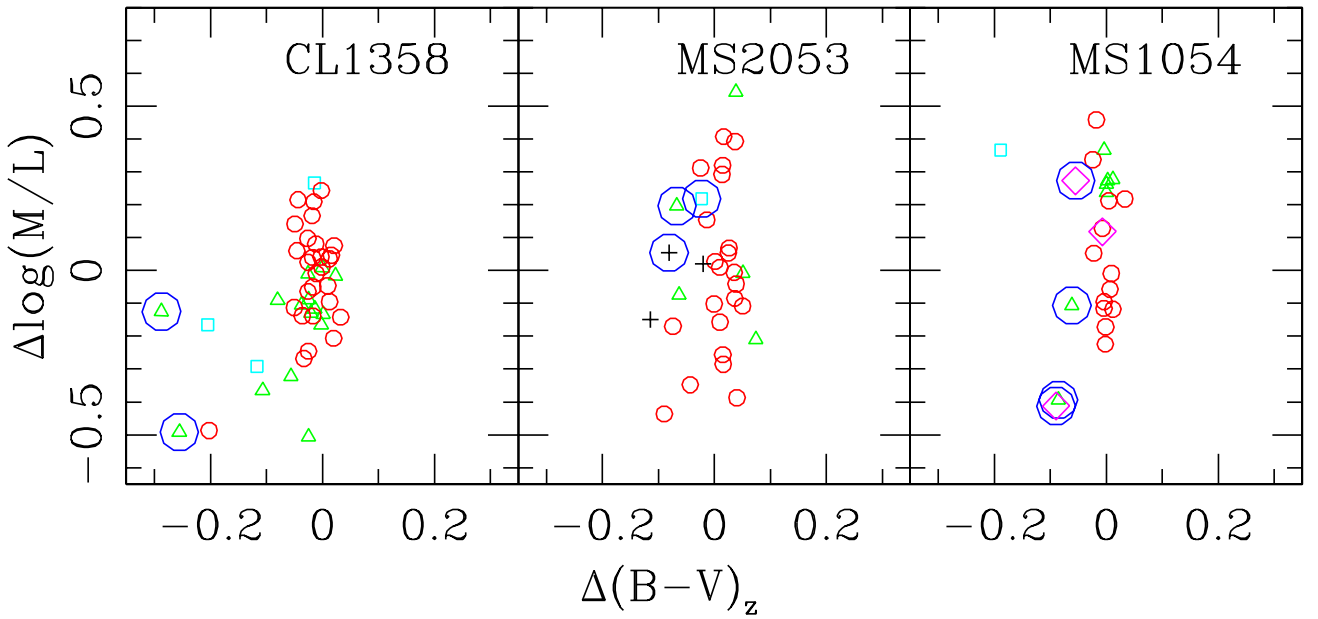


FIG. 8.— The $\log(M/L)$ residuals from the FP plotted against residuals from the $(B - V)_z$ color-magnitude relation for members with measured internal velocity dispersions; the symbols are as in Fig. 3. We estimate cluster galaxies are brightened by as much as ~ 1.25 mag in M_{Be} , with a median of 0.25 mag.

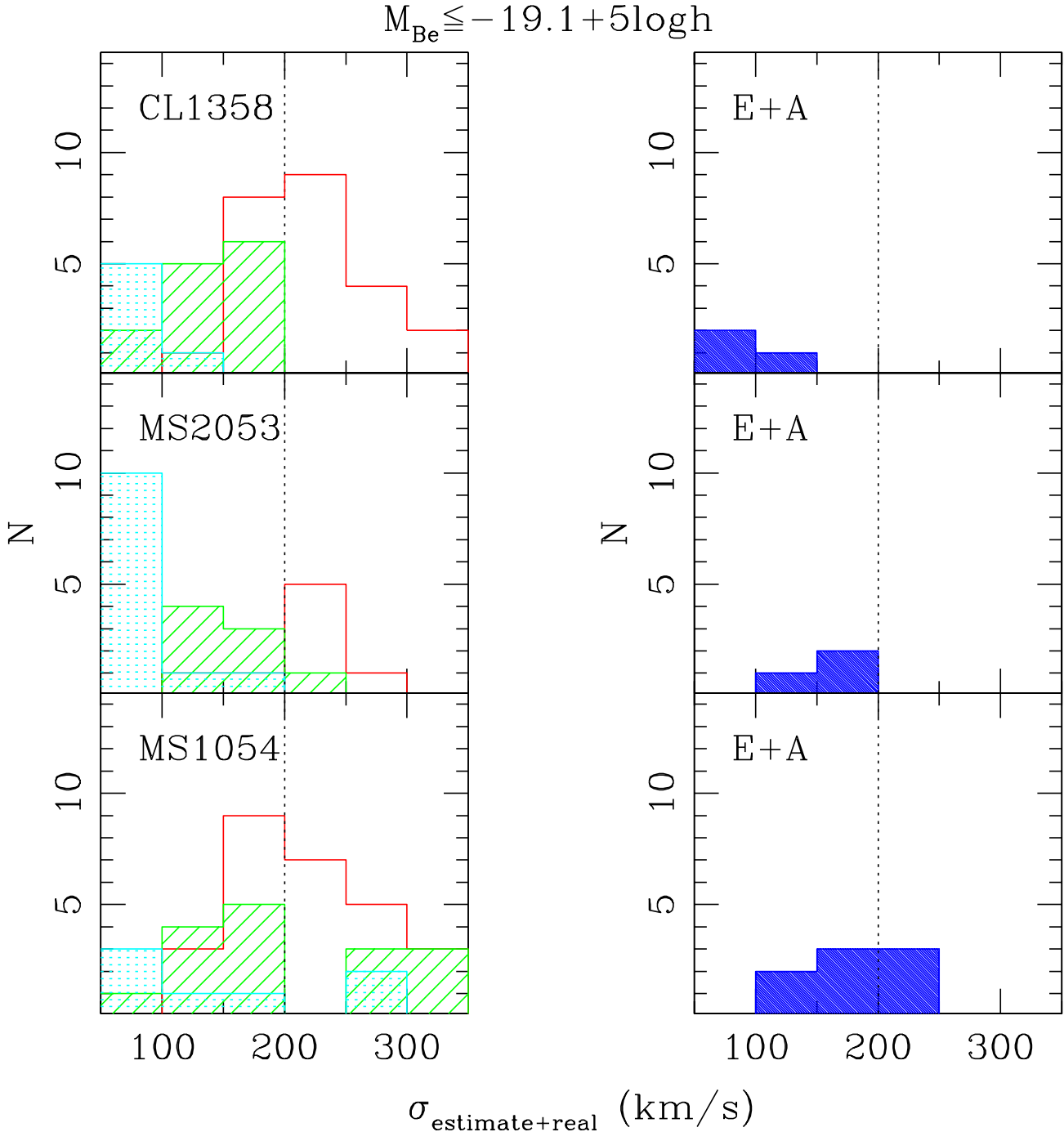


FIG. 9.— Histogram of internal velocity dispersions (measured and estimated) for members brighter than our magnitude limit. In the left panels, open regions correspond to E-S0's ($-5 \leq T \leq -1$), hatched regions to S0/a-Sa's ($0 \leq T \leq 1$), and dotted regions to spirals ($T \geq 2$). The right panels show the respective E+A's that satisfy our strict selection criteria. All of the high σ ($> 200 \text{ km s}^{-1}$; dotted vertical line) members in CL1358 are E-S0's. In contrast, high σ members in MS1054 include S0/a-Sa's, E+A's, spirals, and mergers (not shown).

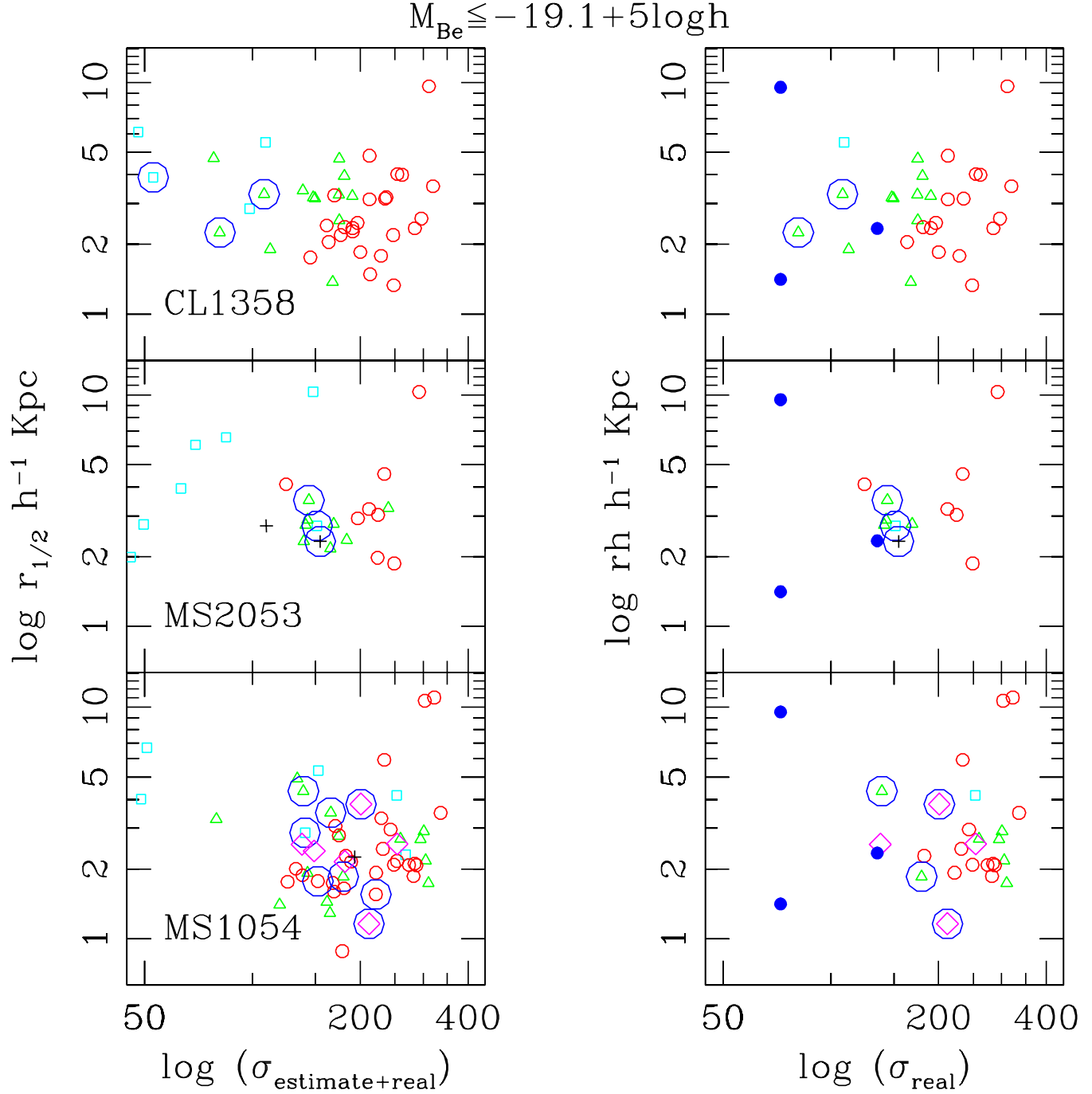


FIG. 10.— Galaxy size, as defined by half-light radius from a de Vaucouleurs bulge+exponential disk model, compared to velocity dispersion for $M_{Be} \leq -19.1 + 5 \log h$ members; both these quantities should be relatively constant with redshift. The symbols are as in Fig. 3. The left panels utilize estimated velocity dispersions (except when actually measured) while only members with measured σ are shown in the right panels. Included in the right panels (solid dots) for comparison are E+A's in Coma; here we use velocity dispersions from Caldwell et al. (1996) and half-light radii from Scudiego et al. (1998). The high σ E+A's in MS1054 are very likely to be the progenitors of massive early-types at low redshifts. Also note the number of high dispersion ($\sigma > 250 \text{ km s}^{-1}$) S0/a-Sa's (triangles) in MS1054; the only possible counterparts to these systems in CL1358 are E-S0's.

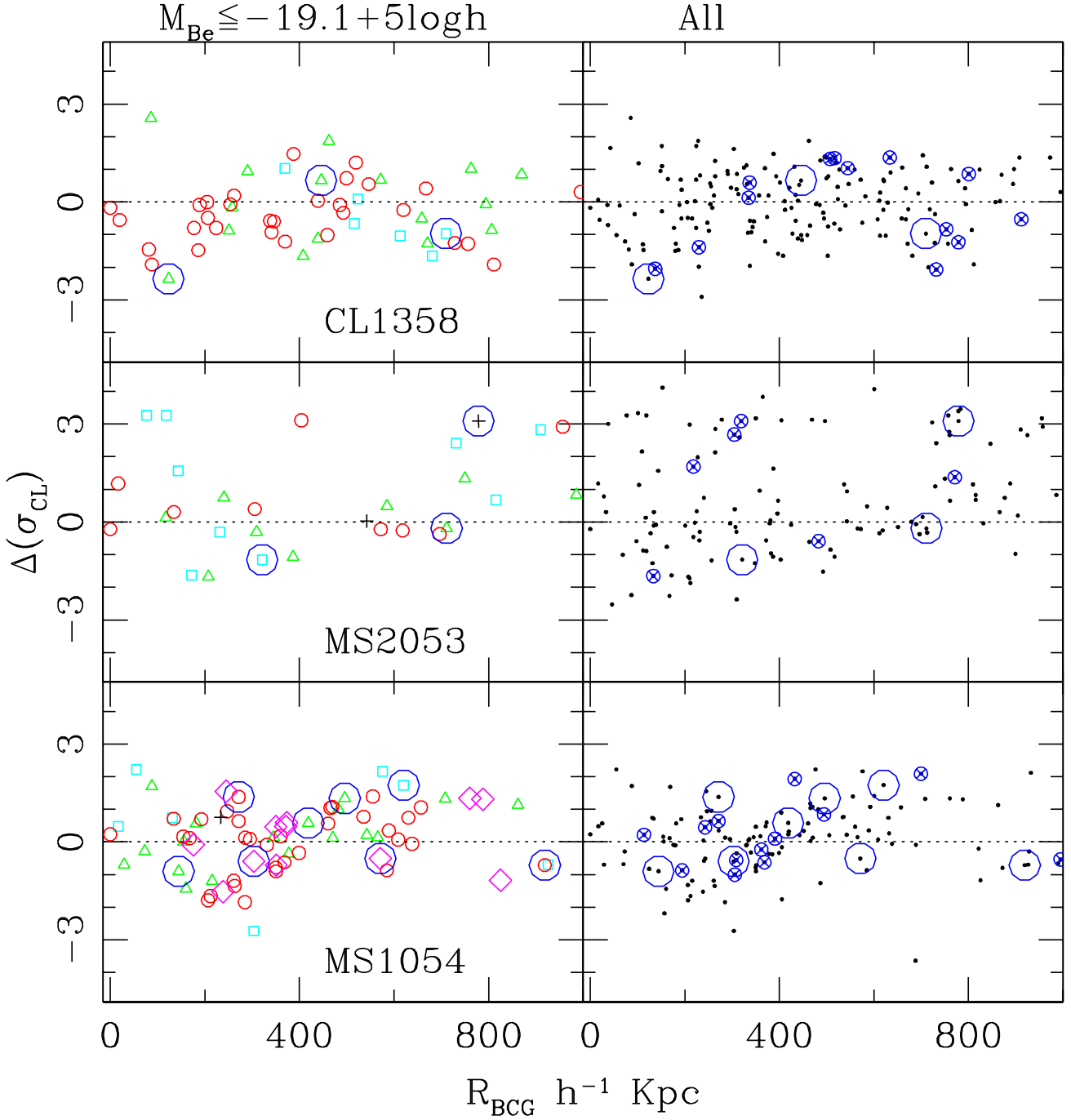


FIG. 11.— Deviation from the cluster's mean velocity dispersion in units of σ_{CL} (the cluster velocity dispersion) for each member. The left panels show only members with $M_{Be} \leq -19.1 + 5\log h$ while the right panels show all confirmed members; the symbols are as in Fig. 3. The large subcluster in MS2053 (Tran 2002) is evident in the middle right panel. In this sample, E+A's are distributed throughout the cluster but none are found at $R_{BCG} < 100h^{-1}$ kpc.

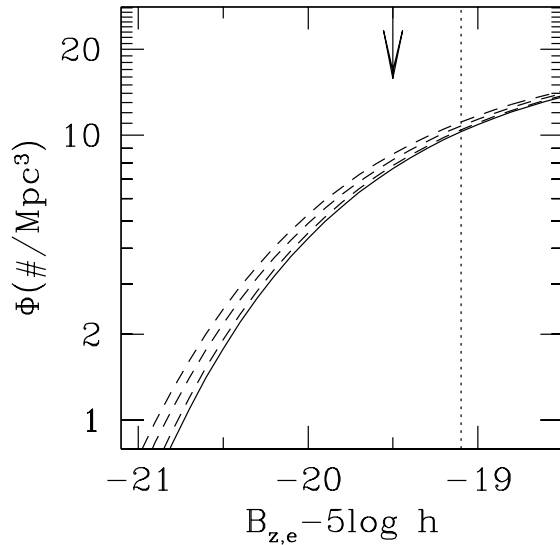


FIG. 12.— How the total luminosity function (solid line) varies when 10, 30, and 50% of the members are brightened by $M_{Be} = 0.25$ mag (dashed lines, increasing from the right); the Φ normalization is arbitrary. The total luminosity function is a combination of a regular distribution ($M_{Be}^* = -19.5 + 5 \log h$; arrow) and a brightened distribution ($M_{Be}^* = -19.75 + 5 \log h$). The dotted vertical line shows our imposed magnitude limit ($M_{Be} = -19.1 + 5 \log h$). Even if only 10% of the members are brightened, the E+A fraction of a luminosity selected sample is $\sim 30\%$ larger than that of a mass selected one.

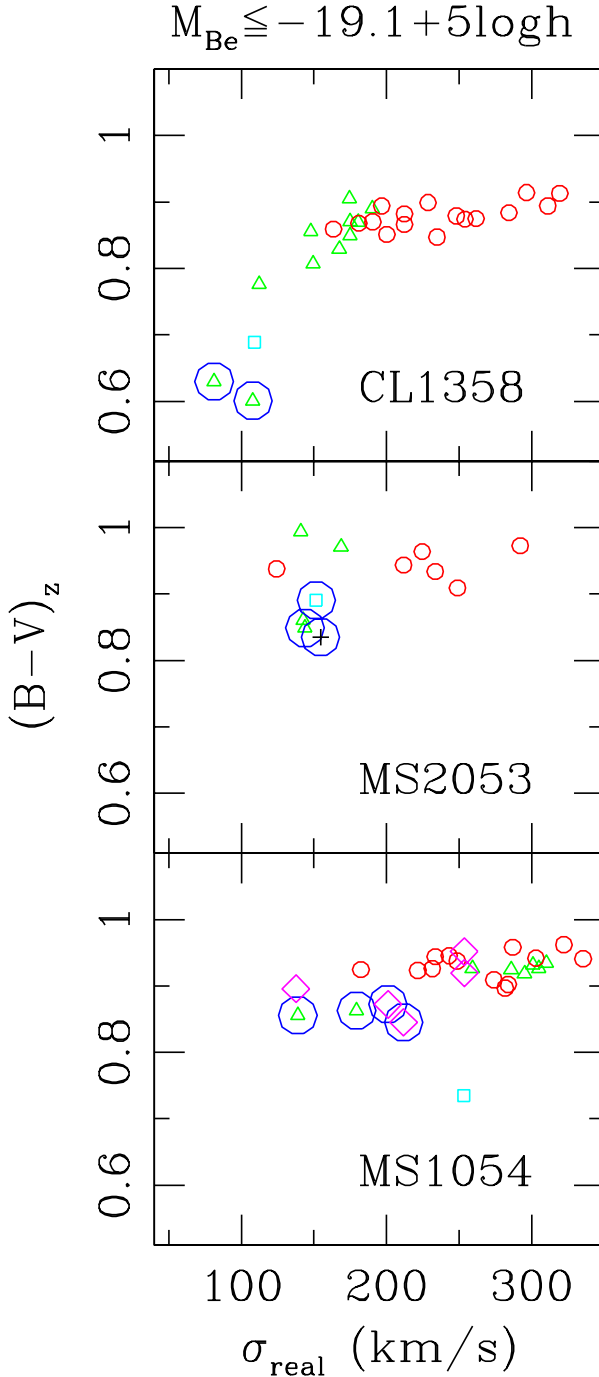


FIG. 13.— Color versus internal velocity dispersion for only cluster members with *measured* dispersions that are brighter than our magnitude limit ($M_{Be} = -19.1 + 5 \log h$). At $z = 0.33$, the only counterparts to the passive, high dispersion ($\sigma > 250 \text{ km s}^{-1}$) S0/a-Sa's (triangles) in MS1054 are E-S0's (small circles). Also note the logical descendants of $\sigma \sim 200 \text{ km s}^{-1}$ E+A's in MS1054 are early-types. Both these points are compelling evidence for morphological evolution in cluster members.

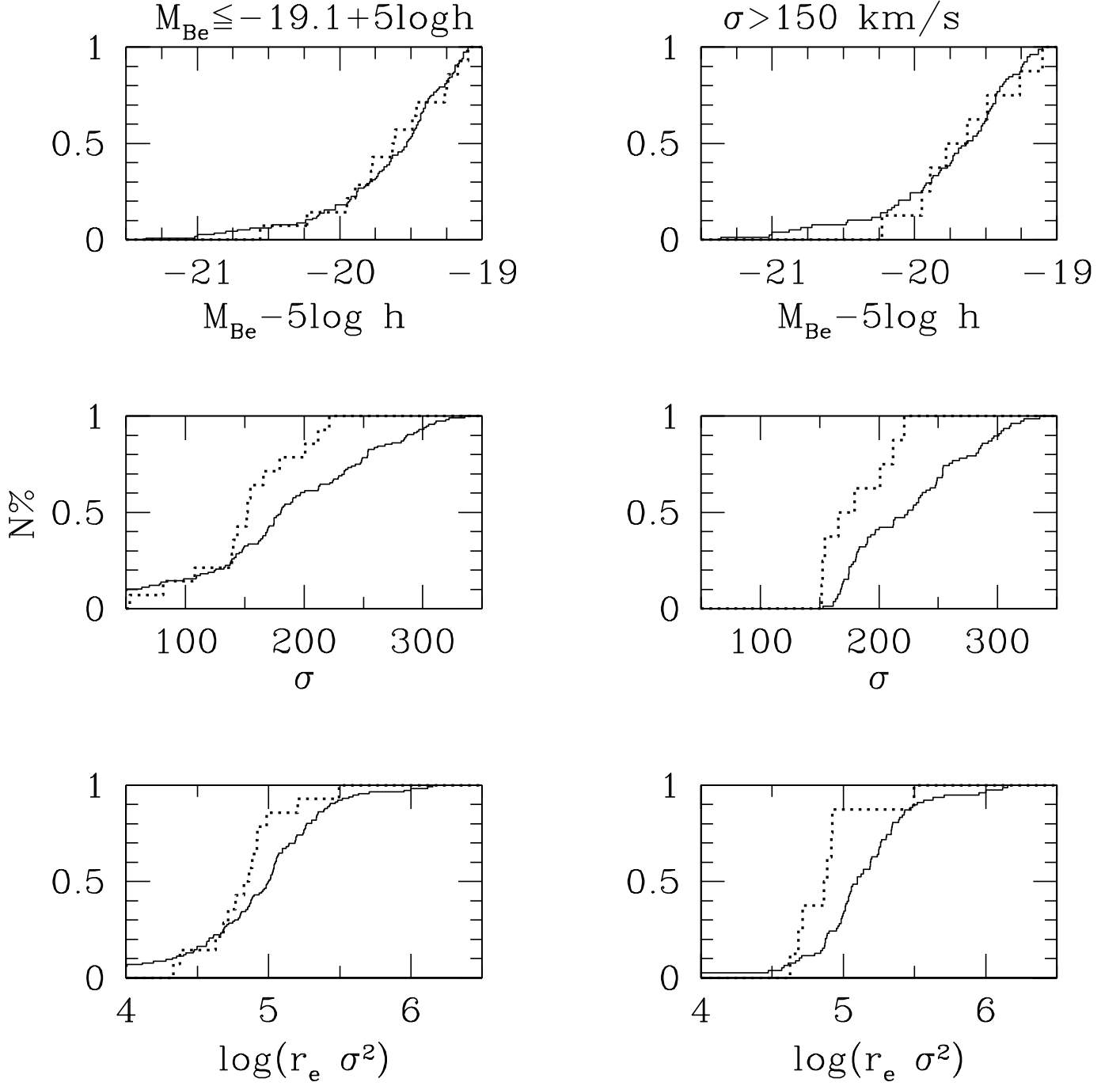


FIG. 14.— *Left Panels*: To determine if the E+A population (dotted lines) differs from the cluster population (solid lines) as a whole, we compare their magnitude (top), internal velocity dispersion (middle), and mass (as traced by $r_e\sigma^2$; bottom) K-S distributions. All three cluster samples are combined to improve the statistics, and we consider only members above our magnitude limit ($M_{Be} = -19.1 + 5\log h$). We find the E+A and cluster M_{Be} distributions are indistinguishable using K-S and Wilcoxon tests. However, the same tests find the σ and mass distributions are different at $\sim 90\%$ CL. Compared to the rest of the spectroscopically confirmed cluster sample, these E+A's tend to have inherently lower velocity dispersions and masses. *Right Panels*: The same analysis except now we apply a velocity dispersion limit ($\sigma > 150 \text{ km s}^{-1}$) in addition to our magnitude cut. Again, we find E+A and cluster M_{Be} distributions to be indistinguishable but their σ and mass distributions differ (both at $> 95\%$ CL).

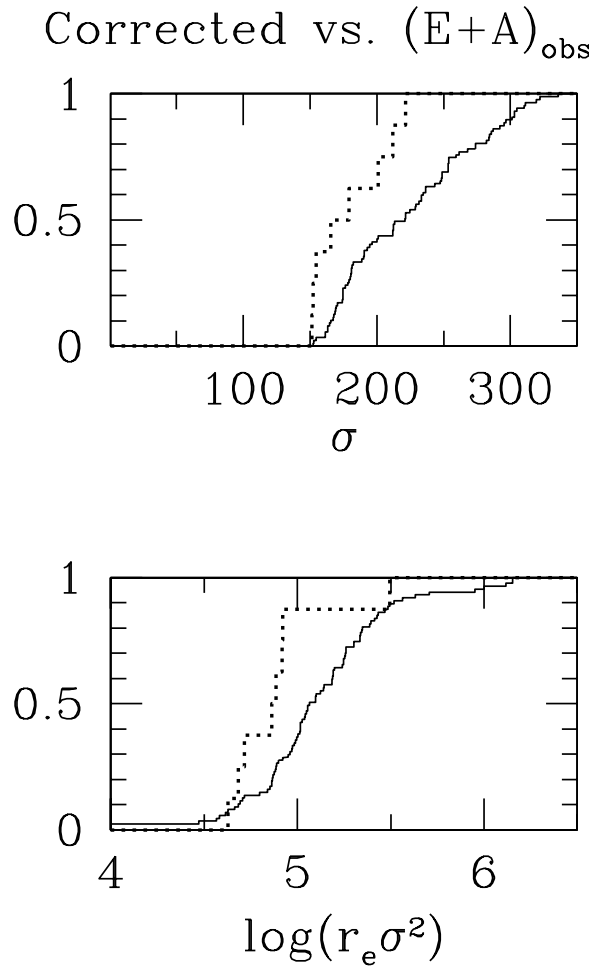


FIG. 15.— We perform a modified K-S test on the observed E+A sample (dotted lines) to the cluster sample (solid lines) corrected for incompleteness ($M_{Be} \leq -19.1 + 5\log h$). We use the combined cluster sample to improve our statistics and consider only galaxies with $\sigma > 150 \text{ km s}^{-1}$. The difference between the E+A's and the other cluster members is significant at the 98% CL for both the internal velocity dispersion and mass ($\propto r_e \sigma^2$) distributions. The significance was derived from Monte Carlo simulations (5000 realizations).

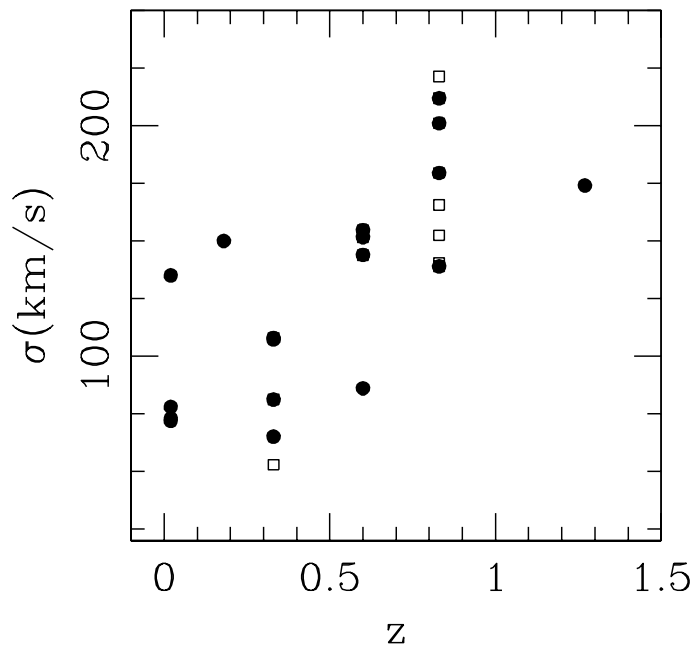


TABLE 1
CLUSTER SAMPLE

Cluster	\bar{z}	$\langle \sigma \rangle_{CL} (\text{km s}^{-1})$	$(m - M)^a$	Reference
CL 1358+62	0.3283 ± 0.0003	1027 ± 50	40.08	Fisher et al. (1998)
MS 2053-04	0.5840 ± 0.0005	870 ± 60	41.31	Tran (2002)
MS 1054-03	0.8309 ± 0.0006	1130 ± 80	42.00	Tran et al. (1999) van Dokkum et al. (2000) Tran (2002)

^aDistance modulus determined using $\Omega_M = 0.3$, $\Omega_\Lambda = 0.7$ cosmology with $H_0 = 100 \text{ km s}^{-1} \text{ Mpc}^{-1}$, and corrected for simple fading as determined from the Fundamental Plane ($\Delta \log(M/L) \propto -0.40z$; van Dokkum et al. 1998a).

TABLE 2
LINE STRENGTH INDEX DEFINITIONS ^a

Index	Bandpass	Blue Sideband	Red Sideband
[OII]	3716.3–3738.3	3696.3–3716.3	3738.3–3758.3
H δ	4083.5–4122.3	4017.0–4057.0	4153.0–4193.0
H γ	4319.8–4363.5	4242.0–4282.0	4404.0–4444.0
H β	4847.9–4876.6	4799.0–4839.0	3738.3–3758.3

^aFrom Fisher et al. (1998).

TABLE 3
E+A SELECTION CRITERIA: CL1358^a

Reference	Balmer (Å) ^b	$\lambda 3727$ (Å) ^b	N^c	Magnitude ^d
Balogh et al. 1999		$H\delta \geq 5$	[OII]>−5	2 $20.0 < m_R < 20.9$
Fisher et al. 1998	$(H\delta + H\gamma + H\beta)/3 \geq 4$		[OII]>−5	4 $20.0 < m_R < 21.4$
Tran 2002 and this paper	$(H\delta + H\gamma)/2 \geq 4$		[OII]>−5	4 $20.0 < m_R < 21.4$

^aConsidering only the 98 members in both F98, B99, and this work.

^bEquivalent widths determining using the bandpasses from Table 2. Absorption is positive, emission is negative.

^cNumber of E+A galaxies using these selection criteria.

^dGunn r magnitudes from the CNOC1 survey (Yee et al. 1996).

TABLE 4
 E+A SAMPLE

Cluster	ID	M_{Be}^a	$(B - V)_z^a$	T-type ^b	$(B/T)^c$	$r_{1/2}$ (kpc) ^{a,c}	$(R_A)^c$	$(R_T)^c$	σ (km s ⁻¹) ^d
CL 1358+62	209*,e	-19.61	0.60	1	0.42	3.3	0.03	0.08	107
	328*	-19.46	0.63	1	0.45	2.3	0.05	0.09	81
	507*	-19.17	0.68	2	0.06	3.9	0.07	0.11	(52)
	343	-18.73	0.67	-2	0.91	1.7	0.01	0.06	65
	92	-18.59	0.85	-2	0.75	1.6	0.02	0.09	(133)
	226	-18.29	0.68	1	0.27	2.9	0.02	0.08	(37)
	109	-18.13	0.67	-2	0.41	1.5	0.01	0.07	(47)
	243	-18.09	0.41	1	0.68	1.6	0.05	-0.02	(23)
	481	-18.04	0.81	-2	0.40	1.8	0.02	0.06	107
	167	-18.01	0.60	-2	0.72	1.8	0.02	0.08	(33)
	I553	-17.81	0.73	5	0.00	1.7	0.03	0.24	(41)
	1775	-17.70	0.80	-4	0.36	2.7	0.04	0.12	(48)
	190	-17.66	0.82	4	0.09	3.1	0.03	0.10	(51)
	565	-17.58	0.68	-2	0.74	1.5	0.00	0.11	(35)
	420	-17.37	0.62	?	0.45	1.7	-0.01	0.04	(24)
	1414	-17.29	0.78	3	0.65	1.5	0.01	0.11	(49)
MS 2053-03	3549*	-19.26	0.84	-897 ^f	0.65	2.3	0.05	0.13	154
	416*	-19.24	0.85	1	0.34	3.5	0.04	0.10	143
	2345*	-19.10	0.89	2	0.33	2.7	0.07	0.09	151
	1746	-18.87	0.58	2	0.46	1.6	0.01	0.10	(38)
	2081	-18.67	0.79	?	0.34	1.8	0.03	0.06	86
	2265	-18.36	0.77	4	0.27	2.5	0.02	0.13	(39)
	1303	-18.22	0.89	3	0.77	3.9	-0.02	0.06	(61)
	1269	-18.00	0.87	-5	0.88	1.0	0.01	0.07	(90)
	408	-17.16	0.56	?	0.03	1.5	0.01	0.00	(13)
	5359*	-20.56	0.86	1	0.07	4.3	0.03	0.06	138
MS 1054-03	5840*	-20.23	0.85	99	1.00	1.2	0.02	0.06	211
	5923*	-19.95	0.84	1	0.41	3.5	0.00	0.05	(165)
	5534*	-19.89	0.81	-5	0.68	1.8	0.01	0.07	(152)
	6567*	-19.78	0.87	99	0.18	3.8	0.04	0.10	201
	2710*	-19.77	0.88	3	0.66	2.9	0.10	0.12	(140)
	2872*	-19.63	0.86	0	0.22	1.9	0.09	0.11	179
	987*	-19.49	0.91	-3	0.39	1.6	0.03	0.13	(221)
	6164	-19.48	0.93	-5	0.69	2.8	0.03	0.04	(174)
	5833	-18.96	0.81	0	0.25	1.8	0.02	0.09	(86)
	5926	-18.72	0.76	0	0.96	1.7	0.01	0.08	(68)
	8001	-18.70	0.85	-5	0.67	0.4	0.01	0.07	(165)
	4390	-18.66	0.93	-4
	5691	-18.61	0.94	0	0.56	1.7	0.03	0.04	(152)
	3356	-18.46	0.79	?	0.92	0.9	0.04	0.10	(79)
	6309	-18.42	0.75	-5	0.45	1.7	-0.01	0.11	(56)
	426	-18.38	0.76	?	0.82	1.2	0.03	0.11	(65)
	2746	-18.09	0.82	?	0.81	1.8	0.05	0.09	(60)
	2467	-17.86	0.81	?	0.96	2.7	0.06	0.15	(60)
	4165	-17.41	0.71	?

TABLE 4—Continued

Cluster	ID	M_{Be}^a	$(B - V)_z^a$	T-type ^b	$(B/T)^c$	$r_{1/2}$ (kpc) ^{a,c}	$(R_A)^c$	$(R_T)^c$	σ (km s ⁻¹) ^d
---------	----	------------	---------------	---------------------	-----------	--------------------------------	-----------	-----------	--

^aThese are E+A galaxies brighter than our magnitude limit of $M_{Be} = -19.1 + 5\log h$ and with Balmer signal to noise flux ratio ≥ 20 .

^aThe galaxy identification numbers used here are from the SExtractor catalogs of the HST/WFPC2 mosaics. We assume an $H_0 = 100h^{-1}$ km s⁻¹Mpc⁻¹, $\Omega_M = 0.3$, $\Omega_\Lambda = 0.7$ cosmology. Redshifted Johnson magnitudes and colors are converted from F606 and F814 fluxes.

^bHubble types are from Fabricant et al. (2000, 2003): E-S0 ($-5 \leq T \leq -1$), S0/a-Sa ($0 \leq T \leq 1$), spirals ($2 \leq T \leq 10$), mergers ($T = 99$), and no type ($T = ?$).

^cStructural parameters are determined from 2D de Vaucouleurs+exponential disk fits in the F814W filter (Tran 2002). Typical systematic errors for B/T , R_A , and R_T are ~ 0.10 , 0.02 , & 0.02 respectively (Im et al. 2001; Tran 2002; Tran et al. 2003).

^dEstimated internal velocity dispersions are noted by ().

^eThis system is not a merger as the two projected cluster members have significantly different redshifts ($\Delta z > 600$ km s⁻¹) from the E+A candidate.

^fGalaxy 2053-3549 has an early-type morphology but there was disagreement between the three classifiers as to its exact Hubble type (Fabricant et al. 2003).

TABLE 5
E+A FRACTIONS

Cluster	N^a	N_{E+A}^a	$F_{E+A}^{a,c}$	n^b	n_{E+A}^b	$f_{E+A}^{b,c}$
CL 1358+62	173	16	$9 \pm 2\%$	42	3	$7 \pm 4\%$
MS 2053-04	132	9	$7 \pm 2\%$	30	3	$10 \pm 6\%$
MS 1054-03	128	20	$16 \pm 3\%$	61	8	$13 \pm 5\%$

^aUsing all spectroscopically confirmed members that fall on the HST/WFPC2 mosaic. We select E+A's as galaxies having $[\text{OII}]\lambda 3727 > -5\text{\AA}$ and $(H\delta + H\gamma)/2 \geq 4\text{\AA}$.

^bConsidering only members above our magnitude cut of $M_{Be} \leq -19.1 + 5\log h$. Robust E+A's are brighter than our magnitude cut and also have H δ and H γ fluxes with high signal to noise ratios (≥ 20).

^cErrors for the E+A fractions are determined by assuming the E+A galaxies follow a Poisson distribution.

APPENDIX

DERIVING GALAXY VELOCITY DISPERSIONS WITH THE FUNDAMENTAL PLANE

The Fundamental Plane (FP, Faber et al. 1987; Djorgovski & Davis 1987) is an empirical relation between galaxy size, surface brightness, and central velocity dispersion. It has the form

$$\log r_e = \alpha \log \sigma + \beta \log I_e + \gamma \quad (\text{A1})$$

where r_e is the effective radius, σ the internal velocity dispersion, I_e the average surface brightness within r_e , and α, β , and γ are measured values. The constants α, β , and γ are determined by applying Eq. A1 to early-type galaxies where all three observables (r_e, σ , and I_e) are known, *e.g.* Jorgensen et al. (1996). Assuming homology, the FP implies that mass to light ratios (M/L) are a function of galaxy mass (Faber et al. 1987).

van Dokkum et al. (1998a) and K00c demonstrated there exists in the FP a tight correlation with little scatter for cluster early-type galaxies up to $z \sim 0.8$. Assuming cluster galaxies evolve passively and do not experience any major mergers, their sizes and internal velocity dispersions do not evolve. We can then exploit this correlation and estimate velocity dispersions from the galaxy's size (r_e) and surface brightness (I_e).

We build on these steps by extending our analysis to include galaxies not observed in K00b. K00c model the stellar populations of the cluster members in CL1358 and assume the residuals of the FP and color-magnitude relation are due to differences in the mean luminosity-weighted ages (Fig. 8). By doing so, K00c find that changes in M/L ratios are strongly correlated with color deviations alone. By correcting M/L ratios of later-type ("bluer") galaxies, we essentially evolve them onto the color-magnitude relation defined by the early-types, *i.e.* these later-types become fainter and redder. We then apply Eq. A1, normalized to the early-type members, to estimate velocity dispersions for the later-type galaxies as well.

Using a stellar population model of constant metallicity and variable age, K00c determine the M/L correction for early-type spirals to be

$$\Delta(M/L_V) = 3.22[\Delta(B - V)]^2 + 3.26\Delta(B - V) \quad (\text{A2})$$

such that the corrected surface brightness is

$$I'_e = I_e \times 10^{3.22[\Delta(B - V)]^2 + 3.26\Delta(B - V)}. \quad (\text{A3})$$

We measure r_e and I_e by fitting *pure de Vaucouleurs* surface brightness profiles to all cluster members; for this profile, $r_e = r_{1/2}$ (Binney & Tremaine 1987). Although E+A's tend to be disk-dominated systems that are not perfectly fit with a pure $r^{1/4}$ profile, we do not expect this to bias our results since Kelson et al. (2000a) showed that the combination of surface brightness and scale-length used in the FP is robust.

From Jorgensen et al. (1996), the measured values of α and β are 1.16 and -0.76 respectively. We determine the normalization γ using the cluster E-S0's for which we have observed values of σ , r_e , and I_e . Velocity dispersions then are estimated for the other cluster members by correcting their surface brightnesses via Eq. A3, and then using I'_e and r_e in Eq. A1 with γ_{E-S0} . For cluster members with measured and estimated velocity dispersions, we find the scatter to be $\sim 20\%$, $\sim 30\%$, and $\sim 35\%$ for CL1358, MS2053, and MS1054 respectively.

This figure "f1a.jpg" is available in "jpg" format from:

<http://arxiv.org/ps/astro-ph/0309460v2>

This figure "f1b.jpg" is available in "jpg" format from:

<http://arxiv.org/ps/astro-ph/0309460v2>

This figure "f2.jpg" is available in "jpg" format from:

<http://arxiv.org/ps/astro-ph/0309460v2>